iScience

CellPress
OPEN ACCESS

Article

Small extracellular vesicles with LncRNA H19 "overload": YAP Regulation as a Tendon Repair Therapeutic Tactic

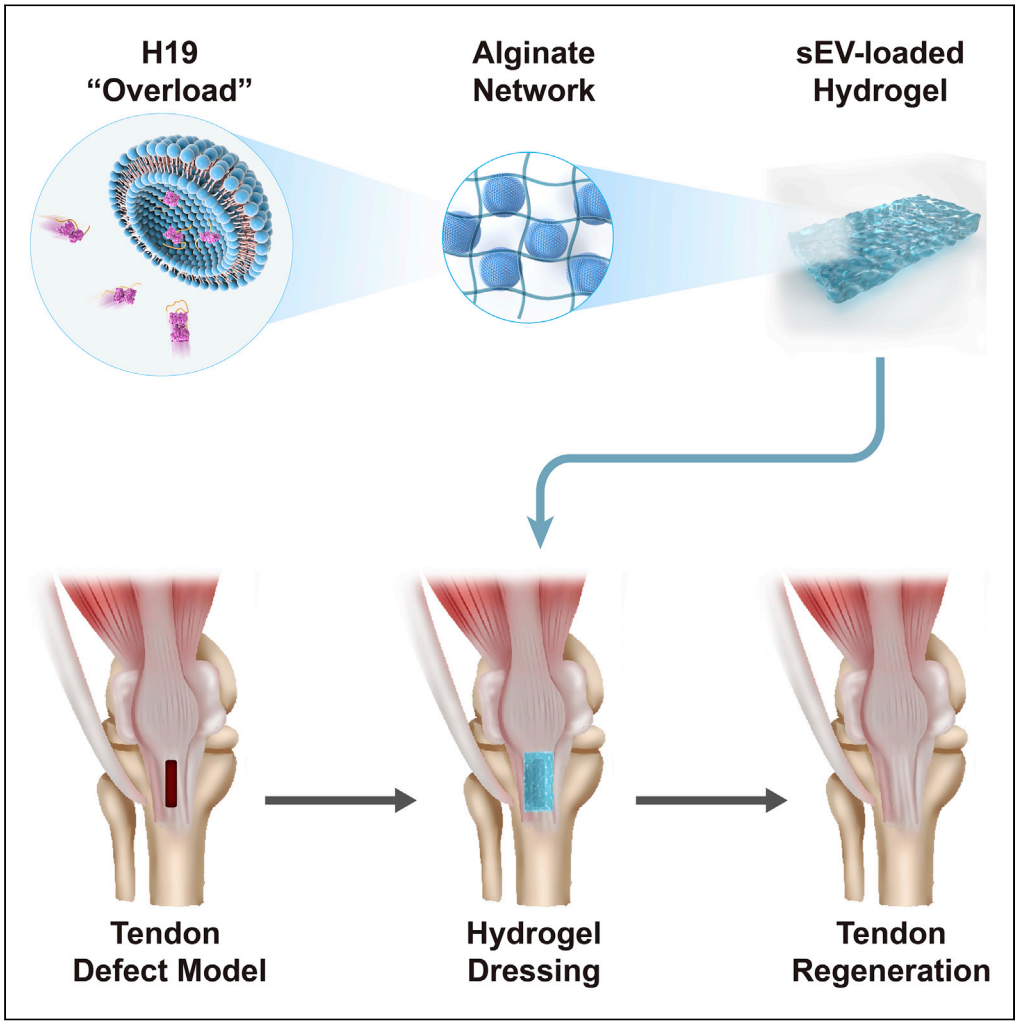

Shi-Cong Tao, Ji-Yan Huang, Zi-Xiang Li, Shi Zhan, Shang-Chun Guo

jerrytao1990@outlook.com (S.-C.T.)
achuni@126.com (S.-C.G.)

HIGHLIGHTS

H19 overexpression enhances tendon regeneration

H19 dephosphorylates and activates YAP

hnRNP A2/B1 assists the enrichment of H19 into sEVs

H19-OL-sEVs promote tendon regeneration

Tao et al., iScience *24*, 102200
March 19, 2021 © 2021 The Author(s).
https://doi.org/10.1016/j.isci.2021.102200

iScience

CellPress
OPEN ACCESS

Article

Small extracellular vesicles with LncRNA H19 "overload": YAP Regulation as a Tendon Repair Therapeutic Tactic

Shi-Cong Tao,[1,*] Ji-Yan Huang,[2] Zi-Xiang Li,[3] Shi Zhan,[4] and Shang-Chun Guo[1,4,5,*]

SUMMARY

Functional healing of tendon injuries remains a great challenge. Small extracellular vesicles (sEVs) have received attention as pro-regenerative agents. H19 overexpression could bring tendon regenerative ability, but the mechanism is still not fully elucidated, and reliable method for delivery of long non-coding RNAs (LncRNAs) was demanded. We identified the downstream mechanism of H19, the activation of yes-associated protein (YAP) via the H19-PP1-YAP axis. We established tendon stem/progenitor cells (TSPCs) stably overexpressing H19 with CRISPR-dCas9-based hnRNP A2/B1 activation (H19-CP-TSPCs). H19-OL-sEVs (H19 "overloading" sEVs) could be produced effectively from H19-CP-TSPCs. Only H19-OL-sEVs were able to significantly load large amounts of H19 rather than other competitors, and the potential of H19-OL-sEVs to promote tendon healing was far better than that of other competitors. Our study established a relatively reliable method for enrichment of LncRNAs into sEVs, providing new hints for modularized sEV-based therapies, and modularized sEVs represented a potential strategy for tendon regeneration.

INTRODUCTION

Tendons are specialized tissues with the primary function of transferring mechanical forces generated by musculoskeletal tissues from muscle to bone. Tendon injury is a common clinical disease that frequently occurs during sports and other rigorous activities, and patients often suffer from long-term pain and even disability (Sharma and Maffulli, 2006). Furthermore, the structural integrity and mechanical strength of damaged tendons rarely attain full recovery or regain native tendon functions after healing because tendons have the characteristics of low oxygen consumption, low metabolism, hypocellularity, and hypovascularity (Sharma and Maffulli, 2006). To date, functional healing of tendon injuries has been a great challenge, and novel therapeutic approaches for tendon regeneration are needed.

Small extracellular vesicles (sEVs), derived from mesenchymal stem cells (MSCs), have become one of the most promising potential therapeutic strategies in tendon regeneration (Zhu et al., 2020). Ongoing research shows that MSC-derived sEVs have many biological functions similar to their parent cells, and they might be the true effectors that play key roles in MSC-based tissue regeneration (Phinney and Pittenger, 2017; Tao et al., 2017b) as well as hold great promise as emerging therapeutic carriers, given their role in intercellular communication (Pi et al., 2018). Our previous study indicated that sEVs derived from native-source cells have various shortcomings (Tao et al., 2017c) and modularized sEVs hold significant promise for targeted and personalized drug delivery (Tao et al., 2018a).

Tendon stem/progenitor cells (TSPCs) were first identified by Bi et al. (2007), who found that they exhibited various common properties of stem cells. TSPCs were shown to display clonogenicity, multilineage differentiation potential, and self-renewal ability (Lee et al., 2015). Therefore, we hypothesized that modularized sEVs, derived from TSPCs, may be desirable promoters of tendon regeneration because of their advantages in accessibility and volume, similar features to tendinocytes, and phenotypic stability.

Recent studies indicated that long non-coding RNA (LncRNA) H19, which was first discovered via genetic screening in 1984 (Pachnis et al., 1984), stimulates tendon regeneration/formation in TSPCs, and that stable overexpression of LncRNA H19 significantly enhances tendon healing (Lu et al., 2017). Compared with

[1]Department of Orthopaedic Surgery, Shanghai Jiao Tong University Affiliated Sixth People's Hospital, 600 Yishan Road, Shanghai 200233, China

[2]Department of Stomatology, Shanghai Shuguang Hospital Affiliated to Shanghai University of Traditional Chinese Medicine, 185 Pu'an Road, Shanghai 200021, China

[3]Department of Medicine, Soochou University, Suzhou, Jiangsu 215123, China

[4]Institute of Microsurgery on Extremities, Shanghai Jiao Tong University Affiliated Sixth People's Hospital, 600 Yishan Road, Shanghai 200233, China

[5]Lead contact

*Correspondence: jerrytao1990@outlook.com (S.-C.T.), achuni@126.com (S.-C.G.)

https://doi.org/10.1016/j.isci.2021.102200

This is an open access article under the CC BY-NC-ND license (http://creativecommons.org/licenses/by-nc-nd/4.0/).

MSC-based therapy, sEV-based therapy is an up-and-coming candidate with lower tumorigenicity and lower immunogenicity (Armstrong et al., 2017; Tao et al., 2018a). TSPCs have been chosen to produce H19-carrying sEVs; however, the efficiency of the conventional approach to load H19 into sEVs is low. In our previous study (Tao et al., 2018b), H19 "loading" was performed through a physical method, like squeezing and pressing, such as using extracellular vesicle-mimetic nanovesicles (EMNVs), which is not a native way to secrete sEVs. A method of improving the efficiency of molecular "loading" through naturally existing mechanisms during EV biogenesis is needed.

RNA content in sEVs is highly selective (Pigati et al., 2010). Human heterogeneous nuclear ribonucleoproteins (hnRNP) A2/B1 are RNA-binding proteins (RBPs) that are known to transport RNA to sEVs (Alarcon et al., 2015) and control RNA loading into sEVs by binding to a motif (Villarroya-Beltri et al., 2013b). H19 is secreted by packaging into sEVs, and this packaging process is reported to be mediated by hnRNP A2/B1 (Lei et al., 2018; Villarroya-Beltri et al., 2013b).

Yes-associated protein (YAP) is involved in the regulation of cell proliferation (Panciera et al., 2017). It is reported that YAP may act as a "switch" between the pro-survival and pro-apoptotic responses (Wu et al., 2015). However, this "switch" remains to be fully characterized. Some studies indicate that the inhibition of YAP (by phosphorylation) down-regulates the expression of tendon-related genes (Chu et al., 2019), whereas activation of YAP (by dephosphorylation) enhances tendon healing (Huang et al., 2020). Therefore, we hypothesized that YAP dephosphorylation might play a crucial role in tendon regeneration.

Proteins can be phosphorylated at serine, threonine, or tyrosine residues, but over 99% of phosphorylation events in mammalian cells involve serine and threonine residues (Mermoud et al., 1992). Protein phosphatase 1 (PP1) is a member of the Ser/Thr-specific protein phosphatase (PP) superfamily. PP1 removes phosphate groups from serine or threonine residues and regulates various cellular processes through the dephosphorylation of dozens of substrates (Grallert et al., 2015). PP1 plays a crucial role in YAP dephosphorylation and regulation (Haemmerle et al., 2017; Lv et al., 2015; Wang et al., 2011).

Many studies have indicated that H19 mediates the interaction between RNA and proteins (Chan et al., 2014; El Hajj et al., 2018). YAP-binding LncRNA screening by RNA immunoprecipitation (RIP) sequencing showed that H19 is one of the top eight candidates (Ni et al., 2019).

In this study, we investigated whether sEVs can be derived from TSPCs by utilizing the co-overexpression of H19 and hnRNP A2/B1, called H19 "overload" sEVs (H19-OL-sEVs), and whether they can promote proliferation, tendon differentiation, migration, collagen deposition, and YAP localization. Our findings will provide a therapeutic exploration of the role of H19-OL-sEVs in tendon regeneration and a better understanding of the regulatory role of H19-PP1-YAP in this process.

RESULTS

Identification of TSPCs and sEVs

TSPC colonies appeared between days 7 and 21 of culture. As observed under the microscope, TSPCs exhibited typical pebble-shaped morphology (Figure 1A). The potential for adipogenic differentiation was studied by measuring the formation of small cytoplasmic lipid granules using oil red O staining after 2 weeks of induction (Figure 1B). Osteogenic differentiation potential was studied by measuring the formation of calcium mineral deposits identified by alizarin red staining after 3 weeks of induction (Figure 1C). The potential for chondrogenic differentiation was analyzed using Alcian blue staining after 4 weeks of induction in alginate beads (Figure 1D). Flow cytometry (FCM) analyses showed that these cells were positive for CD44, CD73, CD90, and CD105 but were negative for CD34 and CD45 (Figure 1E). All these data unequivocally confirmed that TSPCs were successfully isolated from the human tendon.

Morphology of sEVs was examined under a transmission electron microscope (TEM), and particle size distribution was measured using dynamic light scattering (DLS) to identify the sEVs, as shown in Figures 1F and 1G.

Identification of the interaction between H19 and YAP

To further understand the potential biological functions of H19, we investigated H19 expression and found that it was higher in musculoskeletal tissue than in other tissues when analyzed by the data visualization tool of the GTEx database, as shown in Figure 2A.

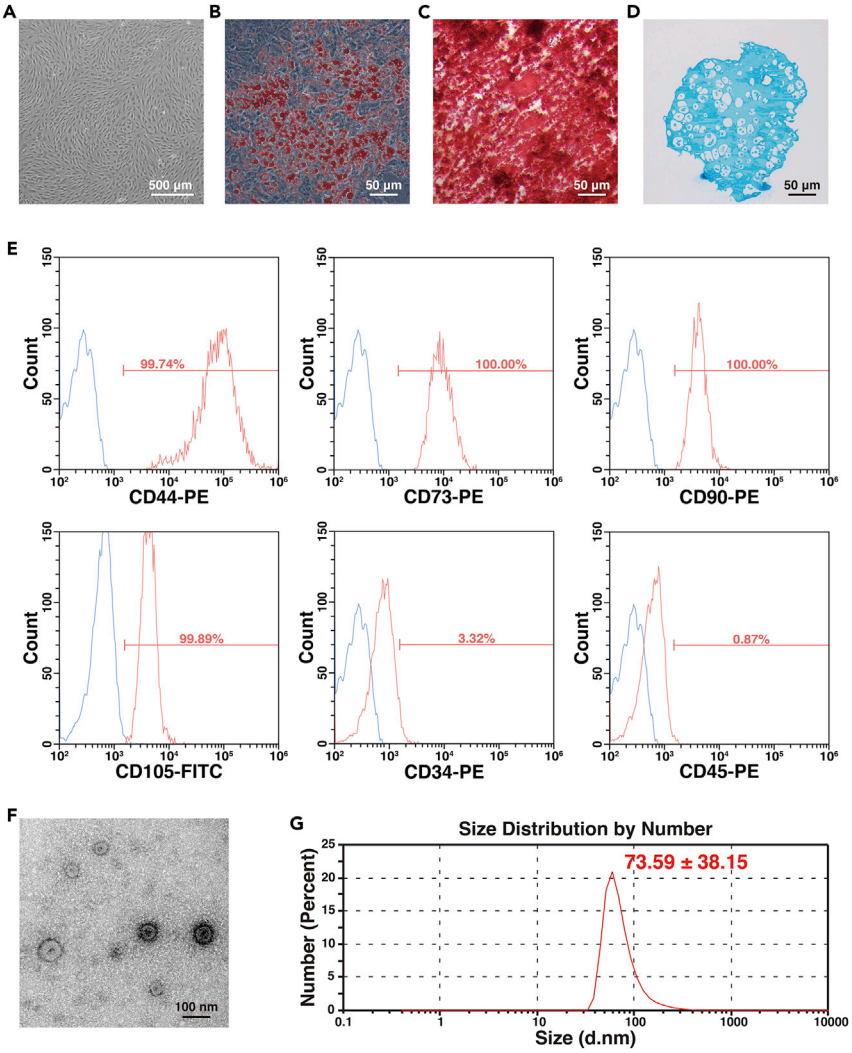

Figure 1. Identification of TSPCs and sEVs

(A) TSPCs exhibited a typical pebble-shaped morphology (scale bar, 500 μm).

(B–D) (B) Adipogenic, (C) osteogenic, and (D) chondrogenic differentiation of TSPCs under induction conditions (scale bar, 50 μm).

(E) Flow cytometry analysis of TSPC cell surface markers. The blue curves represent isotype controls, and the red curves represent measured surface markers (CD44, CD73, CD90, CD105, CD34, and CD45).

(F) Morphology of sEVs under TEM. Scale bar, 100 nm.

(G) The particle size distribution of sEVs measured by DLS. All experiments were repeated independently three times, and representative results are shown. TSPCs, tendon stem/progenitor cells; sEVs, small extracellular vesicles; TEM, transmission electron microscopy.

Moreover, the interaction between *H19* and *YAP* was investigated using the RNA-RNA CoExpression tool of the ENCORI database (starBase v3.0 project). The results showed that YAP downstream genes, such as connective tissue growth factor (*CTGF*), cysteine-rich angiogenic inducer 61 (*CYR61*), and ankyrin repeat domain 1 (*ANKRD1*), were co-expressed (positive correlation) with H19 (Figure 2B).

TSPCs were incubated in the presence of tenogenic induction medium for different periods (t = 0, 3, 5, or 7 days). The expression of *H19*, *YAP* downstream genes (*CYR61*, *CTGF*, and *ANKRD1*), and tenogenic markers (*SCX* and *TNMD*) were assessed via polyacrylamide gel electrophoresis (PAGE) analysis immediately after reverse-transcriptase polymerase chain reaction (RT-PCR) (Figure 2C). The expression level of tenogenic markers were assessed via western blot (WB) analysis (Figure 2D).

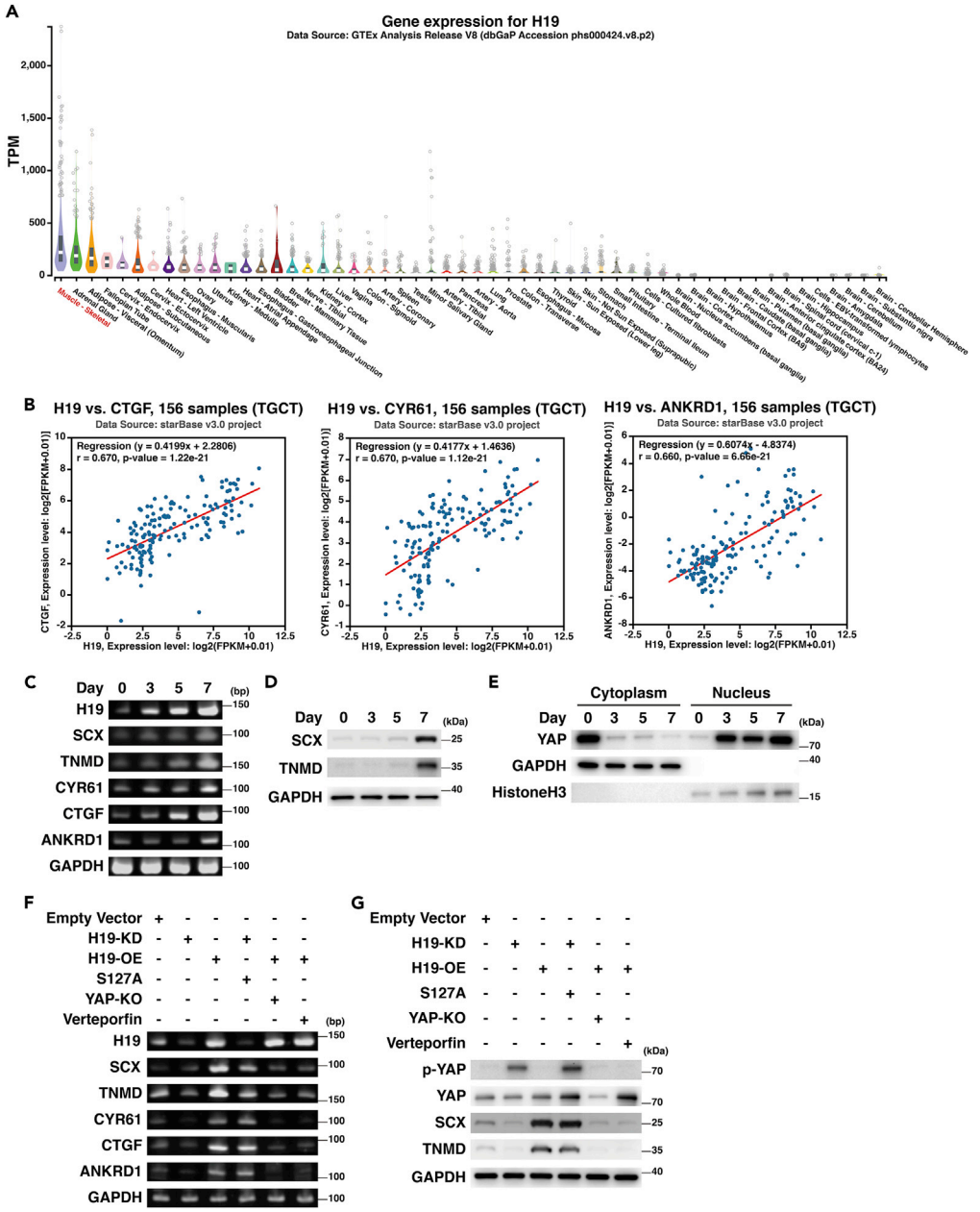

Figure 2. H19 and YAP in tendon regeneration

(A) Expression of *H19* in 54 different tissues from GTEx (v8) datasets, showing that *H19* is highly expressed in musculoskeletal tissue, whereas it is expressed at lower levels in other tissues.

(B) The correlation between H19 and YAP downstream genes (*CTGF*, *Cyr61*, and *ANKRD1*), analyzed via the ENCORI database (starBase v3.0 project).

(C and D) (C) PAGE and (D) western blot analyses were used to measure changes in gene expression during tenogenic differentiation.

(E) YAP cytoplasm-nucleus distribution measured by western blot analysis after nucleus-cytoplasm separate extraction.

(F) Gene expression changes after empty vector, H19-KD, H19-OE, S127A, YAP-KO, and verteporfin treatment.

(G) The phosphorylation level of YAP and expression levels of related proteins were measured by western blot analysis. All experiments were repeated independently three times, and representative results are shown. PAGE, polyacrylamide gel electrophoresis; KD, knockdown; KO, knockout; OE, overexpression; TSPCs, tendon stem/progenitor cells.

Interestingly, there was a positive correlation among *H19*, *YAP* downstream genes, and tenogenic marker genes, measured using PAGE assay (Figure 2C). The endogenous YAP localization is associated with the transcriptional activation of target genes, such as *CTGF* and *CYR61* (Zhao et al., 2010). WB analysis, using cytoplasmic and nuclear protein fractions isolated from TSPCs, further showed that YAP translocation from the cytoplasm to the nucleus followed tenogenic induction/differentiation (Figure 2E).

After treatment with LncRNA-H19 Smart Silencer (H19-KD), pcDNa3.1(+)_A009-H19 (H19-OE), S127A (permanently activated YAP), YAP-KO, or verteporfin (to block the YAP-TEAD interaction), the expression of *H19*, tenogenic marker genes, and *YAP* downstream genes was measured via PAGE analysis (Figure 2F), and the phosphorylation levels of YAP and the expression levels of tenogenic marker genes were detected via WB analysis (Figure 2G). Empty vector was used as a control.

The results showed that H19-KD inhibited YAP activation (by promoting YAP phosphorylation) and YAP downstream processes, as well as the expression of tendon marker genes. In contrast, H19-OE promoted YAP activation (by suppressing YAP phosphorylation) and YAP downstream processes, as well as tendon marker gene expression. S127A rescued cells from the effect of H19-KD, whereas YAP-KO reversed the effect of H19-OE. Verteporfin reversed the H19-OE-induced upregulation of *YAP* downstream and tendon marker genes, without interfering with YAP phosphorylation levels, which implied that H19-induced YAP activation affected tendon marker genes via YAP–TEAD interaction.

Identification of the binding region between H19 and YAP

The results showed that H19 overexpression (H19-OE) or knockdown (H19-KD) did not cause a significant change in the expression and phosphorylation of YAP upstream proteins (MST1/2 and LAST1) (Figure 3A), and this result implied that H19 might have a direct effect on YAP, instead of its upstream regulators. RIP assay was performed to confirm the interaction between H19 and YAP. The results of PAGE showed that H19 was enriched with the YAP antibody compared with the IgG control (Figure 3B). Reciprocally, RNA pull-down and subsequent WB analysis showed that YAP could bind to H19 (Figure 3C). These results suggested that H19 was physically associated with YAP.

To identify the unique binding sites, we took advantage of a series of deletion mutants of H19 to map the YAP-binding region (Figure 3D). Results showed that the H19 mutant Δ3 bound to YAP as efficiently as the full-length H19, whereas other mutants completely lost their binding ability, indicating that nucleotides 780–1210 of H19 are required for its association with YAP.

To identify the YAP regions that are responsible for binding to H19, we constructed four YAP domain-deletion mutants with a hemagglutinin (HA)-tag, and an RNA pull-down assay was performed. Results showed that deletion of the WW domain blocked the interaction, which implied that the WW domain played a critical role in the interaction between YAP and H19 (Figure 3E).

Next, we further used the SWISS-MODEL and RNAstructure software to predict and analyze the 3D structure of the YAP-WW domain and H19 RNA secondary structure, respectively. Figure 3F is a schematic diagram of the YAP–H19 interaction.

H19 regulates PP1-mediated activation of YAP

There are virtually no reports about the direct phosphorylation of LncRNA. Most of the literature suggests that LncRNA can act as a "bridge" between proteins. Hence, we speculated that H19 might form a bridge between YAP and phosphorylated regulatory proteins.

The results of co-immunoprecipitation showed that the binding between PP1 and YAP was significantly decreased when H19 was knocked down and significantly increased when H19 was overexpressed, as shown in Figure S1. However, the binding between PP2 and YAP was changed only a little, independently of the up- or downregulation of H19, and in addition, there were no significant changes in the binding between YAP and MST1/MST2/LATS1 (Figure S1). All these results indicate that H19 acts as a bridge between YAP and PP1.

The phosphorylation level of YAP and the expression level of tenogenic markers were examined via WB analysis upon overexpression or knockdown of H19, as well as PP1α activation (PP1α-ACT) or knockout (PP1α-KO) (Figure 4A). The expression level of H19 and tenogenic markers was examined via PAGE analysis

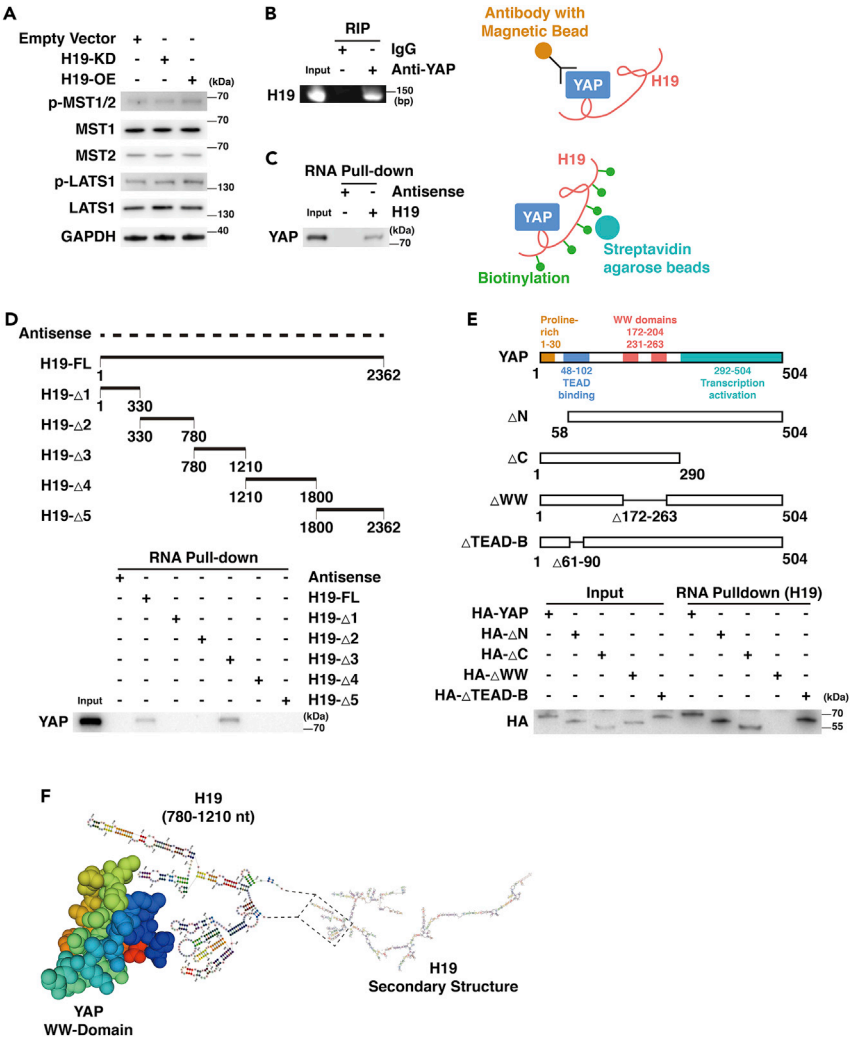

Figure 3. Identification of YAP-H19 interaction

(A) The expression and phosphorylation level of upstream signal molecules of YAP were measured using western blot analysis, after empty vector, H19-KD, and H19-OE treatment.

(B) RNA immunoprecipitation assays for YAP were performed, and H19 was found to be co-precipitated by PAGE analysis.

(C) Western blot analysis after RNA pull-down assay showed the interaction between YAP and H19.

(D) Western blot detection of co-precipitated YAP, which was pulled down by *in vitro*-transcribed biotinylated RNAs corresponding to different fragments of H19 in TSPCs.

(E) Western blot detection of HA-tagged YAP or mutated YAP (wild-type versus domain truncation mutants) co-precipitated with *in vitro*-transcribed biotinylated-H19.

(F) Schematic diagram of the interaction between H19 and YAP. All experiments were repeated independently three times, and representative results are shown. PAGE, polyacrylamide gel electrophoresis; KD, knockdown; KO, knockout; OE, overexpression; TSPCs, tendon stem/progenitor cells.

(Figure 4B). The nucleo-cytoplasmic translocation of YAP was examined via WB analysis (Figure 4C). The results supported our speculation that H19 regulated the phosphorylation level of YAP by acting as a "bridge" between YAP and PP1.

To further visualize the relationship between YAP and PP1, we observed the correlation between YAP and PP1 based on the evidence and data recorded on the GeneMANIA database. Several connections between YAP and PP1 were mapped (Figure 4D). These could be divided into five major sub-clusters based on their biological functions: physical interactions, co-expression, predicted, co-localization, pathway, genetic interactions and shared protein domains. Physical interactions suggested that there were physical

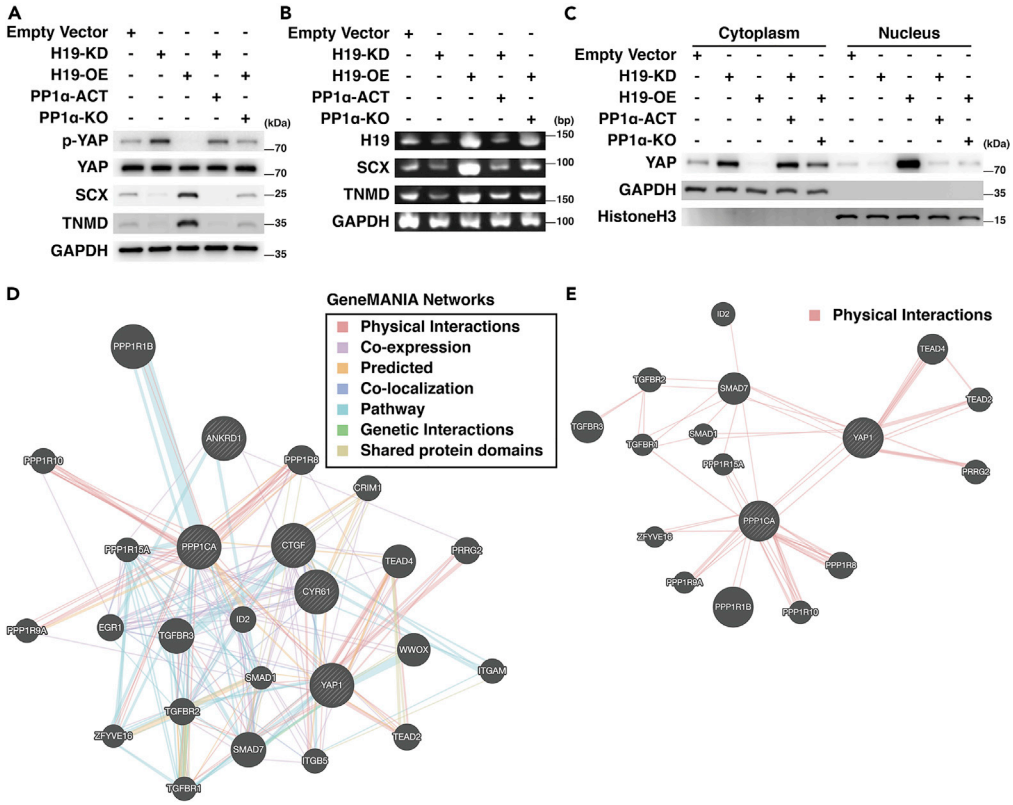

Figure 4. H19 regulates YAP activation mediated by PP1

(A) Western blot analysis showed the levels of total and phosphorylated YAP and tenogenic markers after overexpression or knockdown of H19 with PP1α activation or knockout.

(B) PAGE analysis showed the levels of H19 and tenogenic genes, after overexpression or knockdown of H19 with PP1α activation or knockout.

(C) The nucleo-cytoplasmic translocation of YAP after overexpression or knockdown of H19 with PP1α activation or knockout.

(D) Gene interaction network from GeneMANIA (http://genemania.org/).

(E) Sub-network (physical interactions) from GeneMANIA database (http://genemania.org/). All experiments were repeated independently three times, and representative results are shown. PP1, protein phosphatase 1; PAGE, polyacrylamide gel electrophoresis.

interactions between YAP and PP1 (Figure 4E). Thus, interactions between YAP and PP1 are reliable, and it is meaningful that H19 might be an important regulator of the affinity between YAP and PP1.

H19 regulates the biological functions of TSPCs through PP1-mediated dephosphorylation and translocation of YAP

After treatment with empty vector, H19-KD, H19-OE, H19-KD + S127A, H19-OE + YAP-KO, H19-OE + verteporfin, H19-KD + PP1α-ACT, or H19-OE + PP1α-KO, YAP localization was assessed via immunofluorescence (IF) assay (Figure 5A), proliferation was assessed using the EdU kit and FCM (Figure 5B), and migration was assessed via Transwell assay (Figure 5C).

Collagen deposition was assessed using Sirius red staining after H19-KD, H19-OE, H19-KD + S127A, H19-OE + YAP-KO, H19-OE + verteporfin, H19-KD + PP1α-ACT, or H19-OE + PP1α-KO treatment (Figure 6). The results support our hypothesis that H19 promotes the proliferation, migration, and tendon-related gene expression by regulating YAP phosphorylation and translocation via H19-PP1-YAP interaction.

H19-OL-sEVs regulate the biological function of TSPCs

Expressions of surface markers, including CD9, CD63, and CD81, in cells carrying Con-sEVs (unmodified sEVs), H19-sOE-sEVs (sEVs derived from TSPCs stably over-expressing H19), hnRNP A2/B1-ACT-sEVs

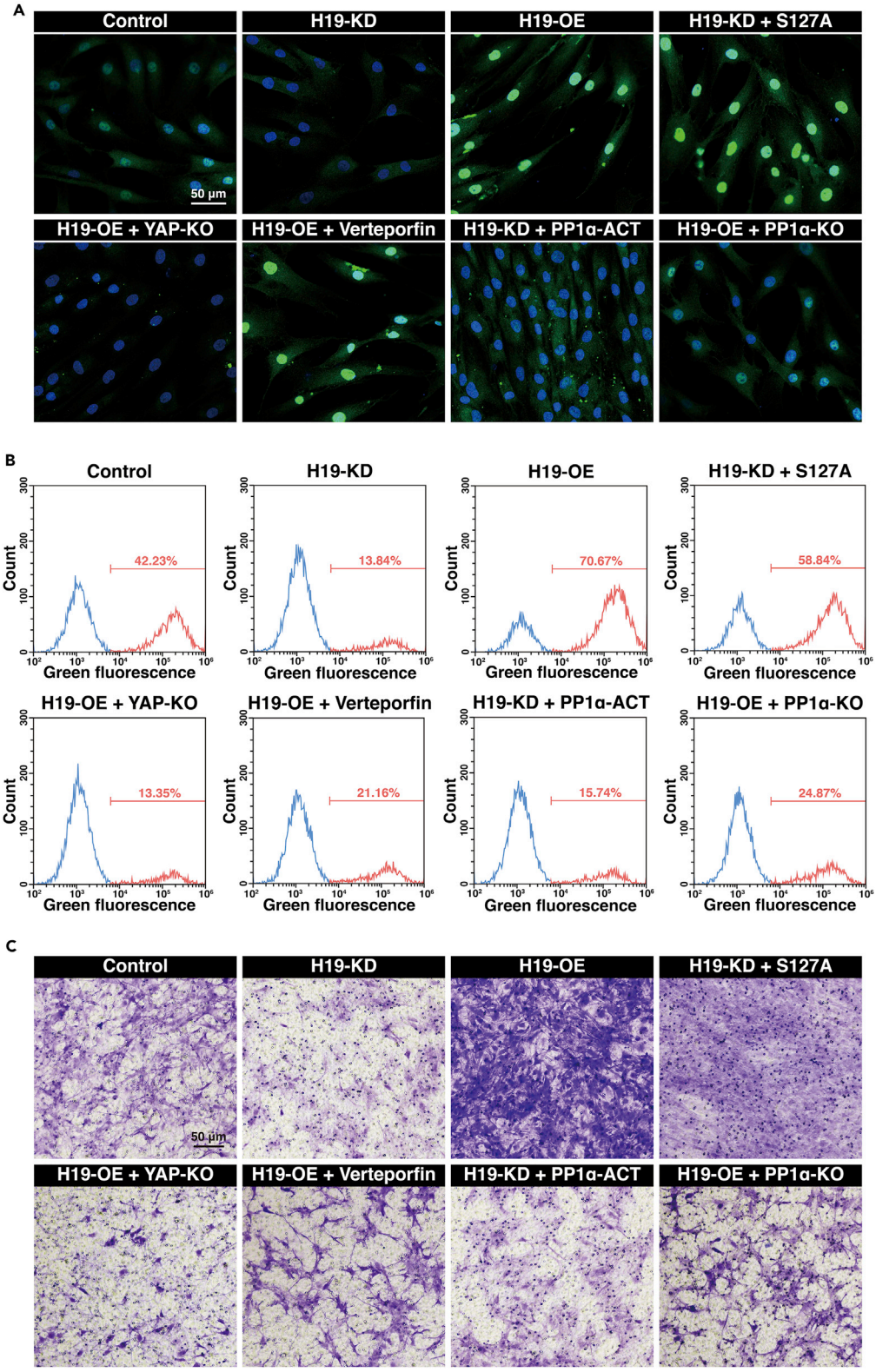
A
Control
H19-KD
H19-OE
H19-KD + S127A
50 μm
H19-OE + YAP-KO
H19-OE + Verteporfin
H19-KD + PP1α-ACT
H19-OE + PP1α-KO
B
Control
H19-KD
H19-OE
H19-KD + S127A
42.23%
13.84%
70.67%
58.84%
H19-OE + YAP-KO
H19-OE + Verteporfin
H19-KD + PP1α-ACT
H19-OE + PP1α-KO
13.35%
21.16%
15.74%
24.87%
Count
Green fluorescence
C
Control
H19-KD
H19-OE
H19-KD + S127A
50 μm
H19-OE + YAP-KO
H19-OE + Verteporfin
H19-KD + PP1α-ACT
H19-OE + PP1α-KO

Figure 5. H19 regulates the biological function of TSPCs through PP1-mediated phosphorylation and degradation of YAP

(A–C) (A) YAP localization was assessed by immunofluorescence assay (scale bar, 50 μm); (B) proliferation was assessed using an EdU kit and flow cytometry, and (C) migration was assessed by Transwell assay (scale bar, 50 μm) after H19-KD, H19-OE, H19-KD + S127A, H19-OE + YAP-KO, H19-OE + verteporfin, H19-KD + PP1α-ACT, or H19-OE + PP1α-KO treatment. All experiments were repeated independently three times, and representative results are shown. KD, knockdown; KO, knockout; OE, overexpression; ACT, activated; TSPCs, tendon stem/progenitor cells; PP1, protein phosphatase 1.

(sEVs derived from TSPCs with hnRNP A2/B1 activation), or H19-OL-sEVs (sEVs derived from TSPCs stably overexpressing H19 with hnRNP A2/B1 activation) were measured using WB and PAGE. The liquid obtained after the same isolation steps from medium in blank wells (without cells) was used as a negative control. This experiment was repeated three times independently, and representative results are shown in Figure 7A. The results support our view that only the overexpression of both H19 and hnRNP A2/B1 at the same time could increase the H19 content in sEVs (we call this phenomenon/technology "overload"). The sEV release curve was shown in Figure S2.

The expression of H19 in TSPCs treated with different groups of sEVs was examined via PAGE assays (Figure 7B). The results further supported the hypothesis that only sEVs with H19 "overload" could significantly upregulate the expression of H19 in receptive cells (TSPCs).

After treatment with Con-sEVs, H19-sOE-sEVs, hnRNP A1/B2-ACT-sEVs, or H19-OL-sEVs, YAP localization was assessed via IF assay (Figure 7C), proliferation was assessed using an EdU kit and FCM (Figure 7D), migration was assessed via Transwell assay (Figure 7E), and tenogenic differentiation and collagen deposition (Figure 7F) were assessed via Sirius red staining. Con-sEVs had little effect on proliferation or migration. H19-sOE-sEVs and hnRNP A1/B2-ACT-sEVs exhibited better biological effects than Con-sEVs. However, H19-OL-sEVs (sEVs with H19 "overload") had a more prominent and significant effect on promoting YAP activation, proliferation, migration, and tenogenic differentiation of TSPCs. Thus, H19-OL-sEVs hold the most promise as a therapeutic agent.

Histological and mechanical properties

In vivo, the effects of H19-OL-sEVs on tendon repair were examined using a rat tendon defect model. During the first 2 weeks post operation, all the skin incision wounds healed with no sign of infections, swelling, or suppuration. Over the 4 weeks post operation, no apparent difference was noticed in any of the animal groups.

After 4 weeks, H&E, Masson's trichrome and Safranin O & Fast green staining indicated that the H19-OL-sEVs group had more matrix and collagen formation in the wound region when compared with the other groups (Figure 8A). All experimental groups had higher cellularity compared with the control group at week 4. Tendon healing occurred extrinsically by the invasion of cells from the surrounding sheath and synovium (Gelberman et al., 1984).

Collagen birefringence was higher in the H19-OL-sEVs group compared with that in other groups at week 4, indicating better collagen fiber alignment (Figure 8A). The collagen birefringence was low in the control group and increased in all other groups. In the H19-OL-sEVs group, collagen fibers with a typical tendon structure were observed. No fibrocartilage or ectopic bone was observed in any of the groups.

At week 4, ultimate stress in the Con-sEVs group was not significantly different compared with the Control group. The ultimate stress in the H19-sOE-sEVs group, hnRNP A2/B1-ACT-sEVs group, and H19-OL-sEVs group was observed to be significantly higher than in the control group, but the ultimate stress in the H19-sOE-sEVs group was not significantly different compared with the Con-sEVs group. The H19-OL-sEVs group showed the most significant recovery of ultimate stress. Young's modulus in the Con-sEVs group was not significantly different compared with the Control group. Meanwhile Young's modulus in the H19-sOE-sEVs, hnRNP A2/B1-ACT-sEVs, and H19-OL-sEVs groups was observed to be significantly higher than in the Control group, but Young's modulus in the H19-sOE-sEVs and hnRNP A2/B1-ACT-sEVs groups was not significantly different compared with Con-sEVs. The H19-OL-sEVs group showed the most significant recovery of Young's modulus. However, there were still significant differences between the normal group and other groups. The statistical results are shown in Figure 8B.

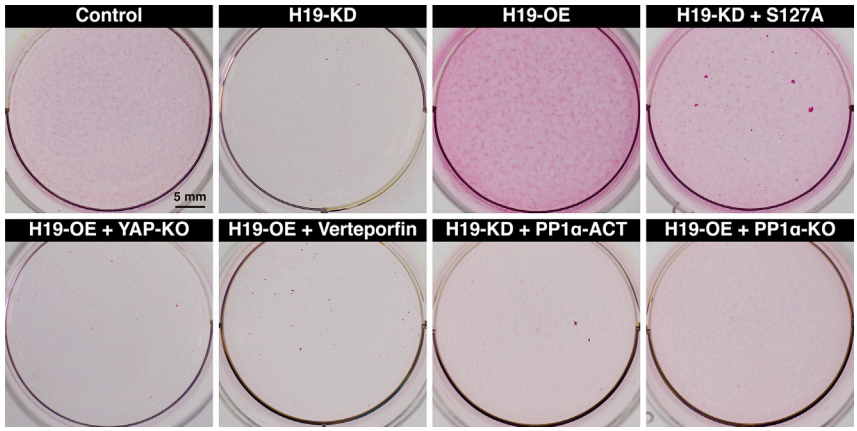

Figure 6. Collagen deposition

Collagen deposition (scale bar, 5 mm) was assessed by Sirius red staining after H19-KD, H19-OE, H19-KD + S127A, H19-OE + YAP-KO, H19-OE + verteporfin, H19-KD + PP1α-ACT, or H19-OE + PP1α-KO treatment. All experiments were repeated independently three times, and representative results are shown. KD, knockdown; KO, knockout; OE, overexpression; ACT, activated.

In addition, we also analyzed dephosphorylation and accumulation of YAP *in vivo* (Figure S3). Con-sEVs group or H19-sOE-sEVs group was not significantly different compared with Control, hnRNP A2/B1-ACT-sEVs group was observed with significant dephosphorylation of YAP (but accumulation of YAP has no statistical difference) compared with the Control, and H19-OL-sEVs group showed the most significant difference compared with Control (both dephosphorylation and accumulation of YAP). The data confirmed that H19-OL-sEVs promoted tendon repair *in vivo*, consistent with the *in vitro* results. Thus H19-OL-sEVs could be a new technique/approach with great potential for tendon regeneration. A diagram showing the proposed mechanism is presented in Figure 9.

DISCUSSION

Tendon may require more than 1 year to recover from injury and may never completely heal (Sharma and Maffulli, 2005), as tendon tissue is not spontaneously repaired. It ultimately forms a mechanically inferior scar-like tissue, and frequently fails to regain the structural integrity, mechanical properties, or functionality of native tendon (Nourissat et al., 2015; Thomopoulos et al., 2003; Voleti et al., 2012). Increased synthesis of collagen is the primary requirement for tendon regeneration. Moreover, cell proliferation, migration, and differentiation at the tendon injury site are the prerequisites for tendon repair (Nourissat et al., 2015). Thus, it is important to find new drugs/molecules, more effective therapeutic targets, and more efficient drug delivery approaches for tendon repair.

Emerging evidence strongly demonstrates that LncRNAs may play important regulatory roles in cell differentiation and tissue regeneration (Loewer et al., 2010). LncRNAs exert their regulatory functions through specific interactions with proteins, including epigenetic modifiers, transcriptional factors/co-activators, and RNP complexes (Xing et al., 2014). LncRNA H19 is one of the most well-known imprinted genes, located on human chromosome 11. It is transcribed only from the maternally inherited allele (Keniry et al., 2012). Under normal physiological conditions, H19 is abundantly expressed in embryonic tissues of endodermal and mesodermal origin and is downregulated after birth in all tissues except skeletal muscle (Lustig et al., 1994), implying its regulatory role in determining the musculoskeletal cell fate.

Recent findings have shown that H19 is an active modulator of musculoskeletal development, promoting osteoblast differentiation of MSCs (Huang et al., 2015), mediating myoblast differentiation and skeletal muscle regeneration (Dey et al., 2014). As the tendon is a crucial component of the musculoskeletal system, it was not surprising that H19 overexpression was found to accelerate tenogenic differentiation *in vitro* and promote tendon repair through cell-based therapy *in vivo* (Lu et al., 2017). Results of the present study strongly suggest that H19 overexpression is an adaptive mechanism in response to a tendon injury, taking into consideration the vital role that H19 plays in cell proliferation.

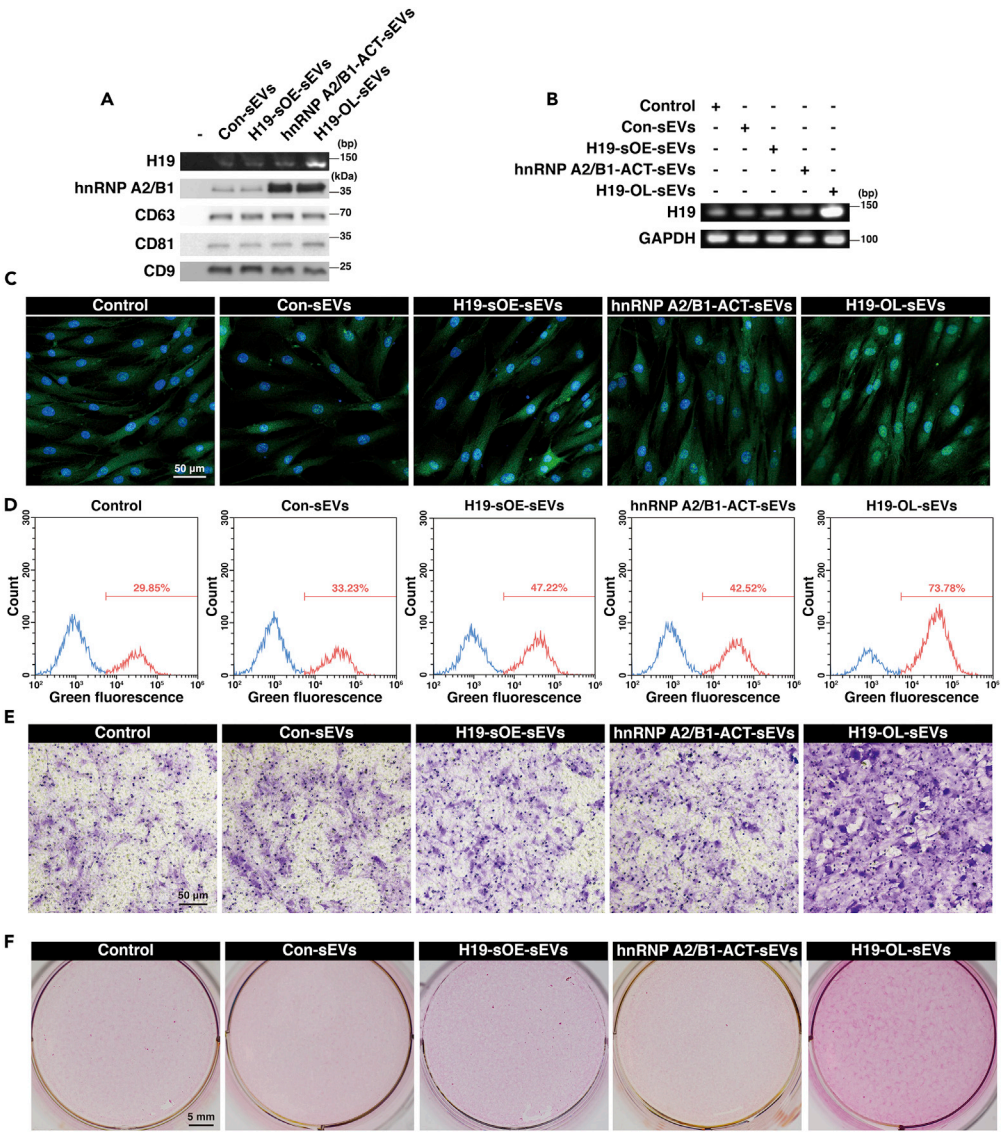

Figure 7. H19-OL-sEVs regulate YAP nuclear localization, proliferation, migration, and collagen deposition in TSPCs

(A) Expressions of surface markers, including CD9, CD63, CD81, in cells carrying Con-sEVs, H19-sOE-sEVs, hnRNP A2/B1-ACT-sEVs, and H19-OL-sEVs were measured using western blotting and PAGE.

(B–F) (B) PAGE assay of H19 expression in TSPCs treated with different groups of sEVs; (C) YAP localization was assessed by immunofluorescence assay (scale bar, 50 μm); (D) proliferation was assessed using an EdU kit and flow cytometry; (E) migration was assessed by Transwell assay (scale bar: 50 μm); (F) collagen deposition was assessed by Sirius red staining (scale bar, 5 mm) after treatment with control, Con-sEVs, H19-sOE-sEVs, hnRNP A1/B2-ACT-sEVs, or H19-OL-sEVs. sEVs, small extracellular vesicles; Con-sEVs, unmodified sEVs; H19-OL-sEVs, H19 "overloading" sEVs; H19-sOE-sEVs, H19-overexpressing sEVs; hnRNP A1/B2-ACT-sEVs, hnRNP A2/B1-activated sEVs; TSPCs, tendon stem/progenitor cells; PAGE, polyacrylamide gel electrophoresis.

Compared with cell-based therapy, sEV-based (or cell-free) therapy is an up-and-coming candidate with lower tumorigenicity and lower immunogenicity (Armstrong et al., 2017; Tao et al., 2018a). In addition, because the regenerative effect of stem cells is based mainly on the autocrine production of growth factors, immunomodulators, and other bioactive molecules carried in sEVs, these structures can be isolated and used instead of cells for a novel therapeutic approach known as "stem cell-based cell-free therapy" (Bacakova et al., 2018). Future directions of research include methods to optimize the therapeutic potential of these stem cells and non-cellular alternatives using EVs.

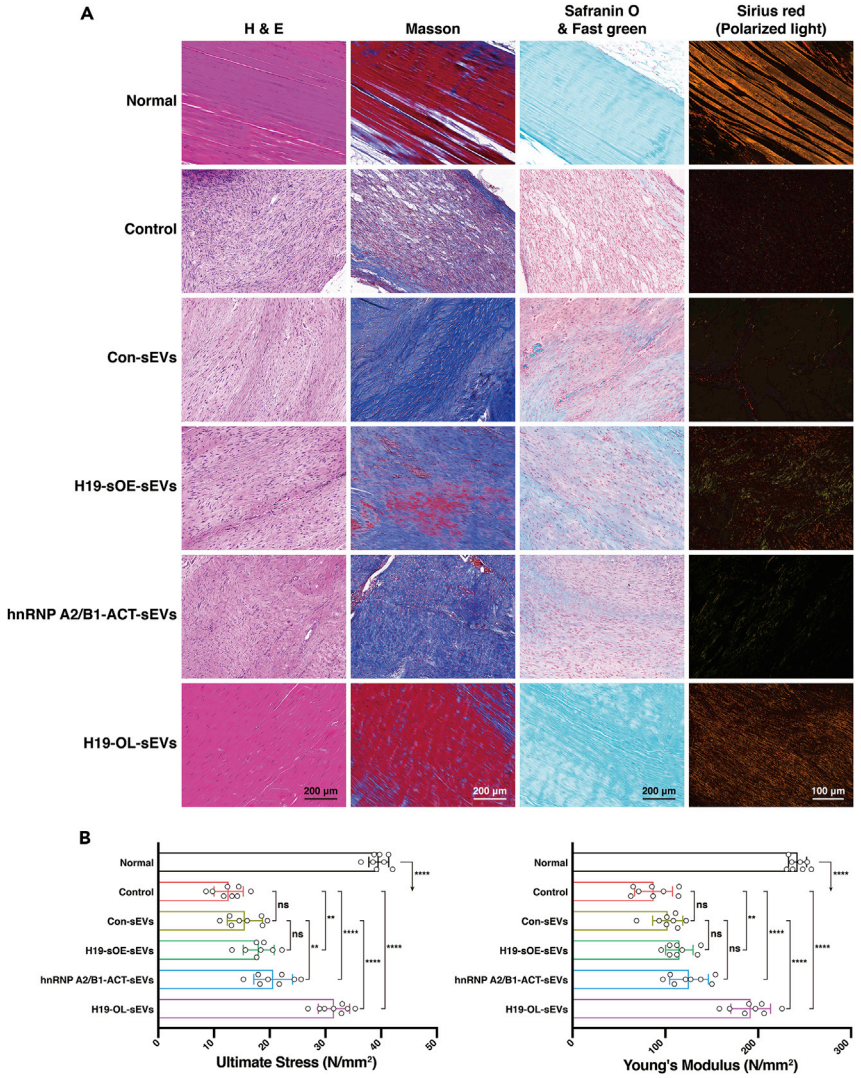

Figure 8. H19-OL-sEVs promotes tendon repair *in vivo*

(A) Histological examination of the effect of different sEV groups on patellar tendon repair detected by H&E (scale bar, 200 μm), Masson's trichrome (scale bar: 200 μm), Safranin O & fast green (scale bar, 200 μm), and Sirius red staining (polarized image) (scale bar, 100 μm).

(B) Statistical charts show the ultimate stress and the Young's modulus in the different groups at week 4 after repair (data are presented as mean ± standard deviation). sEVs, small extracellular vesicles. Significant differences (one-way ANOVA test): ns, no significant difference ($p > 0.05$); **$p < 0.01$; ****$p < 0.0001$.

EVs are small membranous vesicles originating from most, if not all, cells and tissues. Exosomes (or sEVs) are released by various cells (Xia et al., 2019). These membrane-limited vesicles carry multiple cargos, including DNAs, coding or non-coding RNAs, lipids, and proteins, which can be secreted from their parental cells and functionally recruited by recipient cells (Théry et al., 2009), where they can regulate or serve as templates for protein production (Montecalvo et al., 2012). sEVs carry different cargos according to the cell type and probably the physiological state. The transferred molecules are capable of eliciting changes in the function and gene expression of the recipient cell, independent of the recipient cell's location (Lai et al., 2015).

Recently, sEVs, sub-micron vectors used in intercellular communication, have been demonstrated to have exceptional potential as packaging tools for the therapeutic delivery of genetic material and drugs (Armstrong and Stevens, 2018). TSPCs are sEV-releasing cells (Wang et al., 2019), selected as the production

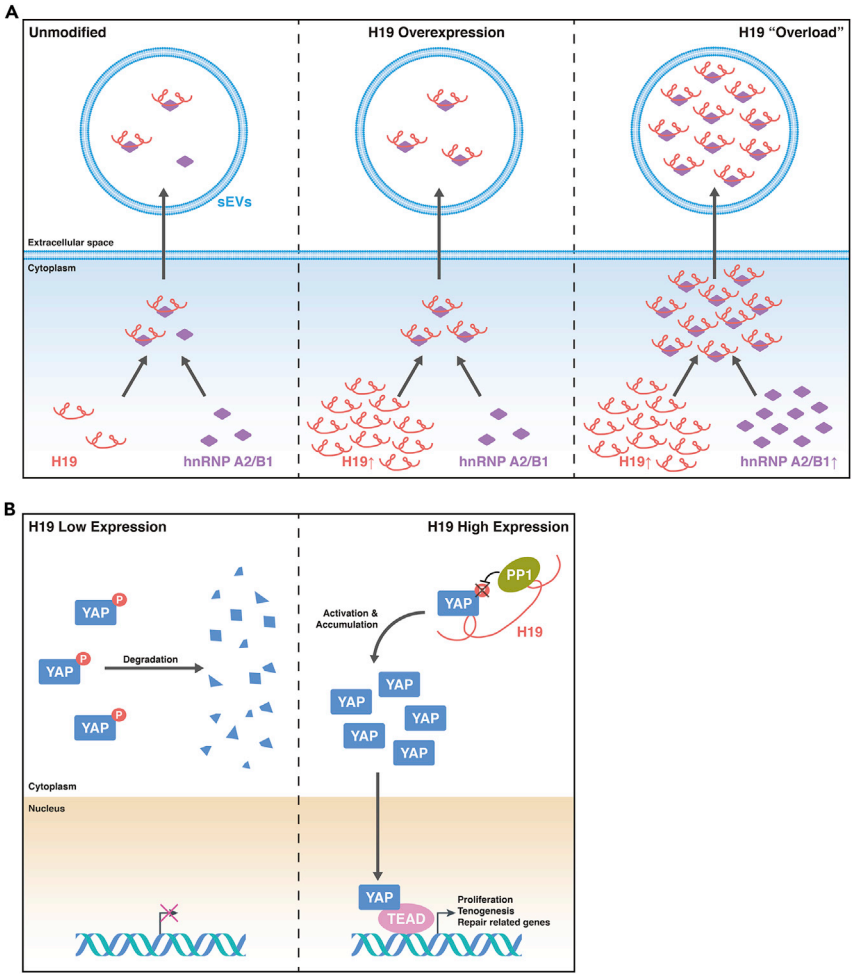

Figure 9. Diagram of the proposed molecular mechanism

(A) Schematic diagram of LncRNA H19 "overload" technology.

(B) Schematic diagram of H19/PP1/YAP interaction, and the mechanisms that enable biological functions.

source of sEVs because they are biologically closer to the repaired tissues, more widely available, and abundant with a broader amplification capacity, less terminal differentiation, and spontaneous tenogenic differentiation potential.

The discovery that sEVs are one of the key secretory products of MSCs, mediating cell-to-cell communication to enhance wound healing, and that cell-derived EV signaling organelles mediate the paracrine effects of stem cells, suggests that cell-free strategies could supplant cell-based therapy (Barile et al., 2017). Because of the relative probability of neoplastic transformation and abnormal differentiation in cell-based therapy, sEVs derived from native-source cells will play a beneficial role in the process of tendon injury and repair (Chamberlain et al., 2019; Shi et al., 2019; Wang et al., 2020). The sEVs derived from tendon stem cells can balance the synthesis and degradation of the tendon extracellular matrix, thus promoting tendon healing (Wang et al., 2019). However, as research progressed, it was realized that sEVs derived from native-source cells may have various shortcomings and show limited pharmaceutical acceptability, which can be corrected via modification and optimization (Tao et al., 2018a). As expected, we demonstrated that H19 participated in tendon regeneration through incorporation into sEVs, using an "overloading" approach.

Emerging evidence indicates that exploitation of EV-based cell-free therapeutics is a promising approach (Das et al., 2019). Much of the recent interest in sEVs was triggered by the discovery of the function of sEVs

in transport of secreted extracellular RNAs (exRNAs), and these exRNAs remain biologically active and functional after they enter the recipient cells (Valadi et al., 2007). We then determined whether the extracellular expression of H19 mediated tenogenic differentiation of TSPCs. Our current study further showed that H19-OL-sEV, a modularized sEV, could promote tendon regeneration when applied as a cell-free therapy instead of a cell-based one. Treatment with H19-OL-sEVs promoted tenogenic differentiation and tendon regeneration, indicating that H19 packaging into sEVs promoted tendon regeneration.

However, the molecular mechanisms underlying specific loading of RNAs into sEVs remain unclear. The discovery of sEVs, as natural delivery tools of functional nucleic acids and proteins, has generated great interest in the drug delivery field, making it possible to harness these vesicles for therapeutic delivery of microRNAs (miRNAs), small interfering RNAs, mRNAs, LncRNAs, peptides, and synthetic drugs (Barile and Vassalli, 2017). Among these functional small RNAs and proteins, miRNAs can be secreted from the parent cells into sEVs through the overexpression of target miRNA to increase their levels (Tao et al., 2017a, 2017c). Overexpression of an miRNA leads to its enrichment in sEVs, and the mechanism that enables the over-representation of short sequence motifs in miRNAs that are commonly enriched in sEVs has been identified (Villarroya-Beltri et al., 2013a).

To solve the problem that larger molecules (including LncRNAs) are difficult to transport through sEVs in large quantities, many scientists hope to develop EMNVs from cells as a superior alternative to natural EVs (Jang et al., 2013). This new form of EV-mimetics is made by breaking down the cells through serial extrusion, using nano-sized filters with diminishing pore sizes. We have previously prepared EMNVs to increase the content of H19 using this method (Tao et al., 2018b). As expected, the load of H19 in these modularized EMNVs was increased, but the mechanism is yet to be clarified. These EMNVs were prepared by mechanically breaking down the cells instead of by natural secretion. This could not be regarded as a superior choice because their long-term adverse effects and precise mechanisms remain to be elucidated.

RBPs are present in sEVs and potentially function in RNA sorting (Mateescu et al., 2017). LncRNAs can be enriched in sEVs with an over-representation of RBP-binding motifs (Ahadi et al., 2016). RBPs are important regulators of many post-transcriptional events, including RNA splicing, transport, and stability. RBPs are likely involved in EV-RNA sorting mechanisms (Mateescu et al., 2017). In mammalian cells, there are over 500 types of RBPs (Gerstberger et al., 2014), and about a quarter of the protein content in EVs is made up of RBPs (Sork et al., 2018). Most of the RNA transfer to specific cellular locations relies on RBPs, which can travel along the cytoskeleton (Di Liegro et al., 2014; Eliscovich et al., 2013). RBPs, including HuR (Mukherjee et al., 2016), hnRNP A2/B1(Villarroya-Beltri et al., 2013a), hnRNPK (Leidal et al., 2020), hnRNPU (Zietzer et al., 2020), and scaffold-attachment factor B1(SAFB) (Leidal et al., 2020), have been found to be involved in RNA packaging into EVs. Most of the current research is focused on the observation of this phenomenon and exploration of the mechanism, but very little research has been done to exploit these mechanisms as a tool for nucleic acid delivery.

The hnRNP A/B proteins are among the smallest but most abundant RBPs, forming the core of the RNP complex that associates with nascent transcripts in eukaryotic cells. These diverse proteins perform a multitude of functions that involve interplays with DNA or, more commonly, RNA (He and Smith, 2009). Like many RBPs belonging to the A/B family, hnRNP A2/B1 plays a variety of key cellular roles, including RNA processing (Villarroya-Beltri et al., 2013a), export, and maintaining stability of its target genes (Goodarzi et al., 2012). HnRNP A2/B1 in sEVs is sumoylated, and this post-translational modification controls hnRNP A2/B1–RNA binding (Villarroya-Beltri et al., 2013a). In addition, hnRNP A2/B1 plays roles in the trafficking of a myriad of cellular RNAs, both from the nucleus to the cytoplasm and from the cytoplasm to EVs (Villarroya-Beltri et al., 2013b).

LncRNAs can be selectively packaged into sEVs, released, and transported to other cells, with subsequent modulation of cellular function (Kogure et al., 2013; Takahashi et al., 2014). Packaging of H19 into sEVs is selective, especially with an increase in EV-associated hnRNP A2/B1 (Lei et al., 2018). The interaction between hnRNP A2/B1 and the microprocessor may represent such selectivity (Alarcon et al., 2015). As H19 can be secreted by packaging into sEVs, mediated by hnRNP A2/B1 (Lei et al., 2018), the overexpression of hnRNP A2/B1 as a carrier is also required to "overload" H19.

To explore this macromolecule overloading technology, we focused on hnRNP A2/B1. Our results showed that sEVs overloaded with H19 with the activation of hnRNP A2/B1 could be released and transferred into

TSPCs. Treatment with H19-OL-sEVs (H19-enriched sEVs) enhanced proliferation, migration, matrix formation, and differentiation of TSPCs.

Although exRNAs have attracted enormous interest, we currently have limited knowledge of the mechanisms that drive and regulate RNA incorporation into sEVs, and of how RNA-encoded messages affect signaling processes in sEV-targeted cells. The biological mechanisms underlying this RNA regulation among EVs remain to be elucidated.

In their latest study, Choi et al. developed an optogenetically engineered exosome system (EXPLOR) for loading a large number of soluble proteins into exosomes via reversible protein-protein interactions controlled by optogenetics (Choi et al., 2020). This is a very enlightening study, because they developed a controllable (by optogenetics) and highly extensible method (a variety of proteins, including RBPs, which could further carry various kinds of RNAs).

Given that tendons mainly function as load-bearing tissues in the musculoskeletal system (Nourissat et al., 2015), YAP is one of the suggested mediators between the mechanical stimulus perceived by the cytoskeleton and the corresponding cellular response (Driscoll et al., 2015). YAP, a component of the nuclear transcriptional complex (Sudol et al., 1995) which is predominantly cytoplasmatic, shuttles from the cytoplasm to the nucleus to activate gene expression (Wan et al., 2018). Importantly, an increase in nuclear YAP is indicative of cell spreading and proliferation (Aragona et al., 2013) but is also correlated with stem cell differentiation (Dupont et al., 2011). The Hippo-YAP signaling pathway is known as a pivotal regulator of organ growth and tissue regeneration (Moya and Halder, 2019). In recent years, there have been an increasing number of regenerative medicine strategies in different organs targeting this pathway (Aharonov et al., 2020; Aloia et al., 2019; Alsamman et al., 2020; Brusatin et al., 2018; Cheung et al., 2020; Gilbert-Honick et al., 2020; Hageman et al., 2020; Li et al., 2020; Sprangers et al., 2020; Zhou et al., 2020). Thus, the Hippo-YAP signaling pathway has great potential and is worthy of further study to better promote the development of regenerative medicine.

Phosphorylation provides an essential mechanism of YAP regulation (inhibition). It has been established that phosphorylation of YAP at Ser127 is involved in the inhibition of YAP by retaining it in the cytoplasm (Basu et al., 2003; Zhao et al., 2007). Phosphorylated YAP remaining in the cytoplasm is degraded and inactivated (Piccolo et al., 2014). YAP is regulated by LATS1/2 or MST1/2 (Ma et al., 2019). However, the results of the present study showed that H19 may directly regulated YAP phosphorylation without the influence of LATS1/2 or MST1/2 (Figure 3A). The de-phosphorylated YAP is localized in the cell nucleus and functions as a transcription co-activator to induce gene expression. Nuclear YAP binds to TEAD and stimulates the transcription of target genes such as CTGF and CYR61 (Zhao et al., 2008).

Our experimental findings suggest a crucial role of H19 in YAP dephosphorylation leading to tendon regeneration. Furthermore, we identified the H19 region that interacts with YAP, located between the nucleotides 780 and 1210 of H19, using deletion mapping. The WW domain of YAP was required for its binding to epigenetic modifiers, such as H19. Through the YAP-WW domain, H19 bound to YAP.

The level of phosphorylation of any protein, such as YAP, depends on the relative activities of protein kinases and PPs. PP1 specifically dephosphorylates the B subunit of phosphorylase kinase, which may link apicobasal polarity to the dephosphorylation of YAP (Ceulemans and Bollen, 2004). Recent studies showed that PP1 dephosphorylates YAP/TAZ *in vitro* (Liu et al., 2011; Wang et al., 2011). The dephosphorylation of YAP by PP1 results in its nuclear accumulation (Wang et al., 2011; Wu et al., 2015). Here, we investigated the connection between YAP activation and the presence of PP1 or PP2A and showed that PP1 is required for H19-mediated YAP activation. Inhibition of PP1 with CRISPR-Cas9 blocked H19-induced dephosphorylation of YAP. Additionally, we found that H19 promoted the interaction between YAP and PP1 as a "bridge." When PP1 was downregulated using CRISPR-Cas9, an increase in H19 had almost no influence on the dephosphorylation of YAP. These results could explain why there is a close association between H19 and tendon regeneration and the ability of YAP to increase proliferation, migration, differentiation, and collagen deposition of TSPCs.

In this study, H19-OL-sEVs showed powerful efficacy to upregulate H19 in recipient cells and promoted tendon regeneration by highly packaging (or "overloading") H19 cargo. Therefore, these modularized

sEVs may be a promising therapeutic approach for the treatment of tendon injuries, and even for future regenerative and tailored medicine.

Limitations of the study

Certainly, there are still some limitations in our current study. In our previous study, we observed H19-induced excessive vascular formation in an angiogenesis model (Tao et al., 2018b). Some researchers reported that angiogenesis might be a double-edged sword—VEGF is conducive to tendon graft maturation and biomechanical strength; however, excess VEGF impedes improvements in biomechanical strength (Takayama et al., 2015). Our study did not go into depth regarding whether there is a threshold or a safe range for VEGF in tendon regeneration. In addition, a previous study on H19, reported by Lu et al., did not find excessive H19-induced vascular formation in tendon tissues (Lu et al., 2017), and we also did not find excessive vascular formation in our study. We considered that H19 might play different roles in different tissues or that the amount used in our study may just be within the safe range, and follow-up studies are needed to further explore the specific mechanism of this phenomenon. In addition, hnRNP A2/B1-ACT-sEVs also showed the second-best therapeutic potential (second only to the H19-OL-sEVs). The reason may be that hnRNP A2/B1 is not a specific carrier of H19, and some other nucleic acid components carrying hnRNP A2/B1 may also play a certain role in our study. However, to determine what other molecules it may be carrying, and what exactly is the function of the nucleic acid components, further research is still needed. In addition, it is also hoped that there will be follow-up studies based on this study to identify a specific H19 carrier in the future.

Resource availability

Lead contact

Further information and requests for resources and reagents should be directed to and will be fulfilled by the lead contact, Shang-Chun Guo (achuni@126.com).

Materials availability

All related information or materials generated in this study are available upon reasonable request.

Data and code availability

The published article includes all data generated in this study.

METHODS

All methods can be found in the accompanying Transparent Methods supplemental file.

SUPPLEMENTAL INFORMATION

Supplemental information can be found online at https://doi.org/10.1016/j.isci.2021.102200.

ACKNOWLEDGMENTS

We are grateful to Prof. Helen Dawes for insightful comments and technical advice. We thank the Shanghai Institute of Biochemistry and Cell Biology, Fudan University, Tongji University, Shanghai University of Traditional Chinese Medicine, and the Animal Experimental Center of Shanghai Sixth People's Hospital for their expert assistance. The present study was supported by the National Natural Science Foundation of China (grant numbers 81301589, 81802226, 81871834, and 82072530), Shanghai Pujiang Programme (grant number 2019PJD038), Shanghai "Rising Stars of Medical Talent" Youth Development Program (Youth Medical Talents – Specialist Program), and Shanghai Jiao Tong University K.C. Wong Medical Fellowship Fund.

AUTHOR CONTRIBUTIONS

S.-C.T. was involved in conceptualization, methodology, validation, provision of resources, project administration, funding acquisition, and writing (reviewing and editing). J.-Y.H., Z.-X.L., and S.Z. were involved in software, formal analyses, data curation, and investigation. S.-C.G. was involved in writing (original draft preparation, reviewing, and editing), provision of resources, funding acquisition, and supervision. All authors read and approved the manuscript and agree to be accountable for all aspects of the research in ensuring that the accuracy or integrity of any part of the work are appropriately investigated and resolved.

DECLARATION OF INTERESTS

The authors declare no conflict of interest.

Received: October 26, 2020
Revised: January 10, 2021
Accepted: February 12, 2021
Published: March 19, 2021

REFERENCES

Ahadi, A., Brennan, S., Kennedy, P.J., Hutvagner, G., and Tran, N. (2016). Long non-coding RNAs harboring miRNA seed regions are enriched in prostate cancer exosomes. Sci. Rep. *6*, 24922.

Aharonov, A., Shakked, A., Umansky, K.B., Savidor, A., Genzelinakh, A., Kain, D., Lendengolts, D., Revach, O.Y., Morikawa, Y., Dong, J., et al. (2020). ERBB2 drives YAP activation and EMT-like processes during cardiac regeneration. Nat. Cell Biol. *22*, 1346–1356.

Alarcon, C.R., Goodarzi, H., Lee, H., Liu, X., Tavazoie, S., and Tavazoie, S.F. (2015). HNRNPA2B1 is a mediator of m(6)A-dependent nuclear RNA processing events. Cell *162*, 1299–1308.

Aloia, L., McKie, M.A., Vernaz, G., Cordero-Espinoza, L., Aleksieva, N., van den Ameele, J., Antonica, F., Font-Cunill, B., Raven, A., Aiese Cigliano, R., et al. (2019). Epigenetic remodelling licences adult cholangiocytes for organoid formation and liver regeneration. Nat. Cell Biol. *21*, 1321–1333.

Alsamman, S., Christenson, S.A., Yu, A., Ayad, N.M.E., Mooring, M.S., Segal, J.M., Hu, J.K., Schaub, J.R., Ho, S.S., Rao, V., et al. (2020). Targeting acid ceramidase inhibits YAP/TAZ signaling to reduce fibrosis in mice. Sci. Transl. Med. *12*, eaay8798.

Aragona, M., Panciera, T., Manfrin, A., Giulitti, S., Michielin, F., Elvassore, N., Dupont, S., and Piccolo, S. (2013). A mechanical checkpoint controls multicellular growth through YAP/TAZ regulation by actin-processing factors. Cell *154*, 1047–1059.

Armstrong, J.P., Holme, M.N., and Stevens, M.M. (2017). Re-engineering extracellular vesicles as Smart nanoscale therapeutics. ACS Nano *11*, 69–83.

Armstrong, J.P.K., and Stevens, M.M. (2018). Strategic design of extracellular vesicle drug delivery systems. Adv. Drug Deliv. Rev. *130*, 12–16.

Bacakova, L., Zarubova, J., Travnickova, M., Musilkova, J., Pajorova, J., Slepicka, P., Kasalkova, N.S., Svorcik, V., Kolska, Z., Motarjemi, H., et al. (2018). Stem cells: their source, potency and use in regenerative therapies with focus on adipose-derived stem cells - a review. Biotechnol. Adv. *36*, 1111–1126.

Barile, L., Moccetti, T., Marbán, E., and Vassalli, G. (2017). Roles of exosomes in cardioprotection. Eur. Heart J. *38*, 1372–1379.

Barile, L., and Vassalli, G. (2017). Exosomes: therapy delivery tools and biomarkers of diseases. Pharmacol. Ther. *174*, 63–78.

Basu, S., Totty, N.F., Irwin, M.S., Sudol, M., and Downward, J. (2003). Akt phosphorylates the Yes-associated protein, YAP, to induce interaction with 14-3-3 and attenuation of p73-mediated apoptosis. Mol. Cell *11*, 11–23.

Bi, Y., Ehirchiou, D., Kilts, T.M., Inkson, C.A., Embree, M.C., Sonoyama, W., Li, L., Leet, A.I., Seo, B.M., Zhang, L., et al. (2007). Identification of tendon stem/progenitor cells and the role of the extracellular matrix in their niche. Nat. Med. *13*, 1219–1227.

Brusatin, G., Panciera, T., Gandin, A., Citron, A., and Piccolo, S. (2018). Biomaterials and engineered microenvironments to control YAP/TAZ-dependent cell behaviour. Nat. Mater. *17*, 1063–1075.

Ceulemans, H., and Bollen, M. (2004). Functional diversity of protein phosphatase-1, a cellular economizer and reset button. Physiol. Rev. *84*, 1–39.

Chamberlain, C.S., Clements, A.E.B., Kink, J.A., Choi, U., Baer, G.S., Halanski, M.A., Hematti, P., and Vanderby, R. (2019). Extracellular vesicle-educated macrophages promote early achilles tendon healing. Stem Cells *37*, 652–662.

Chan, L.H., Wang, W., Yeung, W., Deng, Y., Yuan, P., and Mak, K.K. (2014). Hedgehog signaling induces osteosarcoma development through Yap1 and H19 overexpression. Oncogene *33*, 4857–4866.

Cheung, P., Xiol, J., Dill, M.T., Yuan, W.C., Panero, R., Roper, J., Osorio, F.G., Maglic, D., Li, Q., Gurung, B., et al. (2020). Regenerative reprogramming of the intestinal stem cell state via hippo signaling suppresses metastatic colorectal cancer. Cell Stem Cell *27*, 590–604.e599.

Choi, H., Kim, Y., Mirzaaghasi, A., Heo, J., Kim, Y.N., Shin, J.H., Kim, S., Kim, N.H., Cho, E.S., In Yook, J., et al. (2020). Exosome-based delivery of super-repressor IκBα relieves sepsis-associated organ damage and mortality. Sci. Adv. *6*, eaaz6980.

Chu, G., Yuan, Z., Zhu, C., Zhou, P., Wang, H., Zhang, W., Cai, Y., Zhu, X., Yang, H., and Li, B. (2019). Substrate stiffness- and topography-dependent differentiation of annulus fibrosus-derived stem cells is regulated by Yes-associated protein. Acta Biomater. *92*, 254–264.

Das, S., Ansel, K.M., Bitzer, M., Breakefield, X.O., Charest, A., Galas, D.J., Gerstein, M.B., Gupta, M., Milosavljevic, A., McManus, M.T., et al. (2019). The extracellular RNA communication consortium: establishing foundational knowledge and technologies for extracellular RNA research. Cell *177*, 231–242.

Dey, B.K., Pfeifer, K., and Dutta, A. (2014). The H19 long noncoding RNA gives rise to microRNAs miR-675-3p and miR-675-5p to promote skeletal muscle differentiation and regeneration. Genes Dev. *28*, 491–501.

Di Liegro, C.M., Schiera, G., and Di Liegro, I. (2014). Regulation of mRNA transport, localization and translation in the nervous system of mammals (Review). Int. J. Mol. Med. *33*, 747–762.

Driscoll, T.P., Cosgrove, B.D., Heo, S.J., Shurden, Z.E., and Mauck, R.L. (2015). Cytoskeletal to nuclear strain transfer regulates YAP signaling in mesenchymal stem cells. Biophys. J. *108*, 2783–2793.

Dupont, S., Morsut, L., Aragona, M., Enzo, E., Giulitti, S., Cordenonsi, M., Zanconato, F., Le Digabel, J., Forcato, M., Bicciato, S., et al. (2011). Role of YAP/TAZ in mechanotransduction. Nature *474*, 179–183.

El Hajj, J., Nguyen, E., Liu, Q., Bouyer, C., Adriaenssens, E., Hilal, G., and Segal-Bendirdjian, E. (2018). Telomerase regulation by the long non-coding RNA H19 in human acute promyelocytic leukemia cells. Mol. Cancer *17*, 85.

Eliscovich, C., Buxbaum, A.R., Katz, Z.B., and Singer, R.H. (2013). mRNA on the move: the road to its biological destiny. J. Biol. Chem. *288*, 20361–20368.

Gelberman, R.H., Manske, P.R., Vande Berg, J.S., Lesker, P.A., and Akeson, W.H. (1984). Flexor tendon repair in vitro: a comparative histologic study of the rabbit, chicken, dog, and monkey. J. Orthop. Res. *2*, 39–48.

Gerstberger, S., Hafner, M., Ascano, M., and Tuschl, T. (2014). Evolutionary conservation and expression of human RNA-binding proteins and their role in human genetic disease. Adv. Exp. Med. Biol. *825*, 1–55.

Gilbert-Honick, J., Iyer, S.R., Somers, S.M., Takasuka, H., Lovering, R.M., Wagner, K.R., Mao, H.Q., and Grayson, W.L. (2020). Engineering 3D skeletal muscle primed for neuromuscular regeneration following volumetric muscle loss. Biomaterials *255*, 120154.

Goodarzi, H., Najafabadi, H.S., Oikonomou, P., Greco, T.M., Fish, L., Salavati, R., Cristea, I.M., and Tavazoie, S. (2012). Systematic discovery of structural elements governing stability of mammalian messenger RNAs. Nature *485*, 264–268.

Grallert, A., Boke, E., Hagting, A., Hodgson, B., Connolly, Y., Griffiths, J.R., Smith, D.L., Pines, J., and Hagan, I.M. (2015). A PP1-PP2A phosphatase

relay controls mitotic progression. Nature *517*, 94–98.

Haemmerle, M., Taylor, M.L., Gutschner, T., Pradeep, S., Cho, M.S., Sheng, J., Lyons, Y.M., Nagaraja, A.S., Dood, R.L., Wen, Y., et al. (2017). Platelets reduce anoikis and promote metastasis by activating YAP1 signaling. Nat. Commun. *8*, 310.

Hageman, J.H., Heinz, M.C., Kretzschmar, K., van der Vaart, J., Clevers, H., and Snippert, H.J.G. (2020). Intestinal regeneration: regulation by the microenvironment. Dev. Cell *54*, 435–446.

He, Y., and Smith, R. (2009). Nuclear functions of heterogeneous nuclear ribonucleoproteins A/B. Cell. Mol. Life Sci. *66*, 1239–1256.

Huang, Y., Pan, M., Shu, H., He, B., Zhang, F., and Sun, L. (2020). Vascular endothelial growth factor enhances tendon-bone healing by activating Yes-associated protein for angiogenesis induction and rotator cuff reconstruction in rats. J. Cell. Biochem. *121*, 2343–2353.

Huang, Y., Zheng, Y., Jia, L., and Li, W. (2015). Long noncoding RNA H19 promotes osteoblast differentiation via TGF-beta1/Smad3/HDAC signaling pathway by deriving miR-675. Stem Cells *33*, 3481–3492.

Jang, S.C., Kim, O.Y., Yoon, C.M., Choi, D.S., Roh, T.Y., Park, J., Nilsson, J., Lötvall, J., Kim, Y.K., and Gho, Y.S. (2013). Bioinspired exosome-mimetic nanovesicles for targeted delivery of chemotherapeutics to malignant tumors. ACS Nano *7*, 7698–7710.

Keniry, A., Oxley, D., Monnier, P., Kyba, M., Dandolo, L., Smits, G., and Reik, W. (2012). The H19 lincRNA is a developmental reservoir of miR-675 that suppresses growth and Igf1r. Nat. Cell Biol. *14*, 659–665.

Kogure, T., Yan, I.K., Lin, W.L., and Patel, T. (2013). Extracellular vesicle-mediated transfer of a novel long noncoding RNA TUC339: a mechanism of intercellular signaling in human hepatocellular cancer. Genes Cancer *4*, 261–272.

Lai, C.P., Kim, E.Y., Badr, C.E., Weissleder, R., Mempel, T.R., Tannous, B.A., and Breakefield, X.O. (2015). Visualization and tracking of tumour extracellular vesicle delivery and RNA translation using multiplexed reporters. Nat. Commun. *6*, 7029.

Lee, C.H., Lee, F.Y., Tarafder, S., Kao, K., Jun, Y., Yang, G., and Mao, J.J. (2015). Harnessing endogenous stem/progenitor cells for tendon regeneration. J. Clin. Invest. *125*, 2690–2701.

Lei, Y., Guo, W., Chen, B., Chen, L., Gong, J., and Li, W. (2018). Tumor-released lncRNA H19 promotes gefitinib resistance via packaging into exosomes in non-small cell lung cancer. Oncol. Rep. *40*, 3438–3446.

Leidal, A.M., Huang, H.H., Marsh, T., Solvik, T., Zhang, D., Ye, J., Kai, F., Goldsmith, J., Liu, J.Y., Huang, Y.H., et al. (2020). The LC3-conjugation machinery specifies the loading of RNA-binding proteins into extracellular vesicles. Nat. Cell Biol. *22*, 187–199.

Li, Y., Feng, J., Song, S., Li, H., Yang, H., Zhou, B., Li, Y., Yue, Z., Lian, H., Liu, L., et al. (2020). gp130 controls cardiomyocyte proliferation and heart regeneration. Circulation *142*, 967–982.

Liu, C.Y., Lv, X., Li, T., Xu, Y., Zhou, X., Zhao, S., Xiong, Y., Lei, Q.Y., and Guan, K.L. (2011). PP1 cooperates with ASPP2 to dephosphorylate and activate TAZ. J. Biol. Chem. *286*, 5558–5566.

Loewer, S., Cabili, M.N., Guttman, M., Loh, Y.H., Thomas, K., Park, I.H., Garber, M., Curran, M., Onder, T., Agarwal, S., et al. (2010). Large intergenic non-coding RNA-RoR modulates reprogramming of human induced pluripotent stem cells. Nat. Genet. *42*, 1113–1117.

Lu, Y.F., Liu, Y., Fu, W.M., Xu, J., Wang, B., Sun, Y.X., Wu, T.Y., Xu, L.L., Chan, K.M., Zhang, J.F., et al. (2017). Long noncoding RNA H19 accelerates tenogenic differentiation and promotes tendon healing through targeting miR-29b-3p and activating TGF-beta1 signaling. FASEB J. *31*, 954–964.

Lustig, O., Ariel, I., Ilan, J., Lev-Lehman, E., De-Groot, N., and Hochberg, A. (1994). Expression of the imprinted gene H19 in the human fetus. Mol. Reprod. Dev. *38*, 239–246.

Lv, X.B., Liu, C.Y., Wang, Z., Sun, Y.P., Xiong, Y., Lei, Q.Y., and Guan, K.L. (2015). PARD3 induces TAZ activation and cell growth by promoting LATS1 and PP1 interaction. EMBO Rep. *16*, 975–985.

Ma, S., Meng, Z., Chen, R., and Guan, K.L. (2019). The hippo pathway: biology and pathophysiology. Annu. Rev. Biochem. *88*, 577–604.

Mateescu, B., Kowal, E.J., van Balkom, B.W., Bartel, S., Bhattacharyya, S.N., Buzás, E.I., Buck, A.H., de Candia, P., Chow, F.W., Das, S., et al. (2017). Obstacles and opportunities in the functional analysis of extracellular vesicle RNA - an ISEV position paper. J. Extracell. Vesicles *6*, 1286095.

Mermoud, J.E., Cohen, P., and Lamond, A.I. (1992). Ser/Thr-specific protein phosphatases are required for both catalytic steps of pre-mRNA splicing. Nucleic Acids Res. *20*, 5263–5269.

Montecalvo, A., Larregina, A.T., Shufesky, W.J., Stolz, D.B., Sullivan, M.L., Karlsson, J.M., Baty, C.J., Gibson, G.A., Erdos, G., Wang, Z., et al. (2012). Mechanism of transfer of functional microRNAs between mouse dendritic cells via exosomes. Blood *119*, 756–766.

Moya, I.M., and Halder, G. (2019). Hippo-YAP/TAZ signalling in organ regeneration and regenerative medicine. Nat. Rev. Mol. Cell Biol. *20*, 211–226.

Mukherjee, K., Ghoshal, B., Ghosh, S., Chakrabarty, Y., Shwetha, S., Das, S., and Bhattacharyya, S.N. (2016). Reversible HuR-microRNA binding controls extracellular export of miR-122 and augments stress response. EMBO Rep. *17*, 1184–1203.

Ni, W., Yao, S., Zhou, Y., Liu, Y., Huang, P., Zhou, A., Liu, J., Che, L., and Li, J. (2019). Long noncoding RNA GAS5 inhibits progression of colorectal cancer by interacting with and triggering YAP phosphorylation and degradation and is negatively regulated by the m(6)A reader YTHDF3. Mol. Cancer *18*, 143.

Nourissat, G., Berenbaum, F., and Duprez, D. (2015). Tendon injury: from biology to tendon repair. Nat. Rev. Rheumatol. *11*, 223–233.

Pachnis, V., Belayew, A., and Tilghman, S.M. (1984). Locus unlinked to alpha-fetoprotein under the control of the murine raf and Rif genes. Proc. Natl. Acad. Sci. U S A *81*, 5523–5527.

Panciera, T., Azzolin, L., Cordenonsi, M., and Piccolo, S. (2017). Mechanobiology of YAP and TAZ in physiology and disease. Nat. Rev. Mol. Cell Biol. *18*, 758–770.

Phinney, D.G., and Pittenger, M.F. (2017). Concise review: MSC-derived exosomes for cell-free therapy. Stem Cells *35*, 851–858.

Pi, F., Binzel, D.W., Lee, T.J., Li, Z., Sun, M., Rychahou, P., Li, H., Haque, F., Wang, S., Croce, C.M., et al. (2018). Nanoparticle orientation to control RNA loading and ligand display on extracellular vesicles for cancer regression. Nat. Nanotechnol. *13*, 82–89.

Piccolo, S., Dupont, S., and Cordenonsi, M. (2014). The biology of YAP/TAZ: hippo signaling and beyond. Physiol. Rev. *94*, 1287–1312.

Pigati, L., Yaddanapudi, S.C., Iyengar, R., Kim, D.J., Hearn, S.A., Danforth, D., Hastings, M.L., and Duelli, D.M. (2010). Selective release of microRNA species from normal and malignant mammary epithelial cells. PLoS One *5*, e13515.

Sharma, P., and Maffulli, N. (2005). Tendon injury and tendinopathy: healing and repair. J. Bone Joint. Surg. Am. *87*, 187–202.

Sharma, P., and Maffulli, N. (2006). Biology of tendon injury: healing, modeling and remodeling. J. Musculoskelet. Neuronal Interact. *6*, 181–190.

Shi, Z., Wang, Q., and Jiang, D. (2019). Extracellular vesicles from bone marrow-derived multipotent mesenchymal stromal cells regulate inflammation and enhance tendon healing. J. Transl. Med. *17*, 211.

Sork, H., Corso, G., Krjutskov, K., Johansson, H.J., Nordin, J.Z., Wiklander, O.P.B., Lee, Y.X.F., Westholm, J.O., Lehtiö, J., Wood, M.J.A., et al. (2018). Heterogeneity and interplay of the extracellular vesicle small RNA transcriptome and proteome. Sci. Rep. *8*, 10813.

Sprangers, J., Zaalberg, I.C., and Maurice, M.M. (2020). Organoid-based modeling of intestinal development, regeneration, and repair. Cell Death Differ. *28*, 95–107.

Sudol, M., Bork, P., Einbond, A., Kastury, K., Druck, T., Negrini, M., Huebner, K., and Lehman, D. (1995). Characterization of the mammalian YAP (Yes-associated protein) gene and its role in defining a novel protein module, the WW domain. J. Biol. Chem. *270*, 14733–14741.

Takahashi, K., Yan, I.K., Haga, H., and Patel, T. (2014). Modulation of hypoxia-signaling pathways by extracellular linc-RoR. J. Cell Sci. *127*, 1585–1594.

Takayama, K., Kawakami, Y., Mifune, Y., Matsumoto, T., Tang, Y., Cummins, J.H., Greco, N., Kuroda, R., Kurosaka, M., Wang, B., et al. (2015). The effect of blocking angiogenesis on

anterior cruciate ligament healing following stem cell transplantation. Biomaterials *60*, 9–19.

Tao, S.C., Guo, S.C., Li, M., Ke, Q.F., Guo, Y.P., and Zhang, C.Q. (2017a). Chitosan wound dressings incorporating exosomes derived from MicroRNA-126-overexpressing synovium mesenchymal stem cells provide sustained release of exosomes and heal full-thickness skin defects in a diabetic rat model. Stem Cell Transl. Med. *6*, 736–747.

Tao, S.C., Guo, S.C., and Zhang, C.Q. (2017b). Platelet-derived extracellular vesicles: an emerging therapeutic approach. Int. J. Biol. Sci. *13*, 828–834.

Tao, S.C., Guo, S.C., and Zhang, C.Q. (2018a). Modularized extracellular vesicles: the dawn of prospective personalized and precision medicine. Adv. Sci. (Weinh) *5*, 1700449.

Tao, S.C., Rui, B.Y., Wang, Q.Y., Zhou, D., Zhang, Y., and Guo, S.C. (2018b). Extracellular vesicle-mimetic nanovesicles transport LncRNA-H19 as competing endogenous RNA for the treatment of diabetic wounds. Drug Deliv. *25*, 241–255.

Tao, S.C., Yuan, T., Zhang, Y.L., Yin, W.J., Guo, S.C., and Zhang, C.Q. (2017c). Exosomes derived from miR-140-5p-overexpressing human synovial mesenchymal stem cells enhance cartilage tissue regeneration and prevent osteoarthritis of the knee in a rat model. Theranostics *7*, 180–195.

Théry, C., Ostrowski, M., and Segura, E. (2009). Membrane vesicles as conveyors of immune responses. Nat. Rev. Immunol. *9*, 581–593.

Thomopoulos, S., Williams, G.R., Gimbel, J.A., Favata, M., and Soslowsky, L.J. (2003). Variation of biomechanical, structural, and compositional properties along the tendon to bone insertion site. J. Orthop. Res. *21*, 413–419.

Valadi, H., Ekström, K., Bossios, A., Sjöstrand, M., Lee, J.J., and Lötvall, J.O. (2007). Exosome-mediated transfer of mRNAs and microRNAs is a novel mechanism of genetic exchange between cells. Nat. Cell Biol. *9*, 654–659.

Villarroya-Beltri, C., Gutiérrez-Vázquez, C., Sánchez-Cabo, F., Pérez-Hernández, D., Vázquez, J., Martin-Cofreces, N., Martinez-Herrera, D.J., Pascual-Montano, A., Mittelbrunn, M., and Sánchez-Madrid, F. (2013a). Sumoylated hnRNPA2B1 controls the sorting of miRNAs into exosomes through binding to specific motifs. Nat. Commun. *4*, 2980.

Villarroya-Beltri, C., Gutierrez-Vazquez, C., Sanchez-Cabo, F., Perez-Hernandez, D., Vazquez, J., Martin-Cofreces, N., Martinez-Herrera, D.J., Pascual-Montano, A., Mittelbrunn, M., and Sanchez-Madrid, F. (2013b). Sumoylated hnRNPA2B1 controls the sorting of miRNAs into exosomes through binding to specific motifs. Nat. Commun. *4*, 2980.

Voleti, P.B., Buckley, M.R., and Soslowsky, L.J. (2012). Tendon healing: repair and regeneration. Annu. Rev. Biomed. Eng. *14*, 47–71.

Wan, S., Fu, X., Ji, Y., Li, M., Shi, X., and Wang, Y. (2018). FAK- and YAP/TAZ dependent mechanotransduction pathways are required for enhanced immunomodulatory properties of adipose-derived mesenchymal stem cells induced by aligned fibrous scaffolds. Biomaterials *171*, 107–117.

Wang, C., Hu, Q., Song, W., Yu, W., and He, Y. (2020). Adipose stem cell-derived exosomes decrease fatty infiltration and enhance rotator cuff healing in a rabbit model of chronic tears. Am. J. Sports Med. *48*, 1456–1464.

Wang, P., Bai, Y., Song, B., Wang, Y., Liu, D., Lai, Y., Bi, X., and Yuan, Z. (2011). PP1A-mediated dephosphorylation positively regulates YAP2 activity. PLoS One *6*, e24288.

Wang, Y., He, G., Guo, Y., Tang, H., Shi, Y., Bian, X., Zhu, M., Kang, X., Zhou, M., Lyu, J., et al. (2019). Exosomes from tendon stem cells promote injury tendon healing through balancing synthesis and degradation of the tendon extracellular matrix. J. Cell. Mol. Med. *23*, 5475–5485.

Wu, H., Wei, L., Fan, F., Ji, S., Zhang, S., Geng, J., Hong, L., Fan, X., Chen, Q., Tian, J., et al. (2015). Integration of Hippo signalling and the unfolded protein response to restrain liver overgrowth and tumorigenesis. Nat. Commun. *6*, 6239.

Xia, X., Wang, Y., Huang, Y., Zhang, H., Lu, H., and Zheng, J.C. (2019). Exosomal miRNAs in central nervous system diseases: biomarkers, pathological mediators, protective factors and therapeutic agents. Prog. Neurobiol. *183*, 101694.

Xing, Z., Lin, A., Li, C., Liang, K., Wang, S., Liu, Y., Park, P.K., Qin, L., Wei, Y., Hawke, D.H., et al. (2014). lncRNA directs cooperative epigenetic regulation downstream of chemokine signals. Cell *159*, 1110–1125.

Zhao, B., Li, L., Lei, Q., and Guan, K.L. (2010). The Hippo-YAP pathway in organ size control and tumorigenesis: an updated version. Genes Dev. *24*, 862–874.

Zhao, B., Wei, X., Li, W., Udan, R.S., Yang, Q., Kim, J., Xie, J., Ikenoue, T., Yu, J., Li, L., et al. (2007). Inactivation of YAP oncoprotein by the Hippo pathway is involved in cell contact inhibition and tissue growth control. Genes Dev. *21*, 2747–2761.

Zhao, B., Ye, X., Yu, J., Li, L., Li, W., Li, S., Yu, J., Lin, J.D., Wang, C.Y., Chinnaiyan, A.M., et al. (2008). TEAD mediates YAP-dependent gene induction and growth control. Genes Dev. *22*, 1962–1971.

Zhou, X., Chen, N., Xu, H., Zhou, X., Wang, J., Fang, X., Zhang, Y., Li, Y., Yang, J., and Wang, X. (2020). Regulation of Hippo-YAP signaling by insulin-like growth factor-1 receptor in the tumorigenesis of diffuse large B-cell lymphoma. J. Hematol. Oncol. *13*, 77.

Zhu, Z., Zhang, Y., Wu, L., Hua, K., and Ding, J. (2020). Regeneration-related functional cargoes in mesenchymal stem cell-derived small extracellular vesicles. Stem Cell Dev. *29*, 15–24.

Zietzer, A., Hosen, M.R., Wang, H., Goody, P.R., Sylvester, M., Latz, E., Nickenig, G., Werner, N., and Jansen, F. (2020). The RNA-binding protein hnRNPU regulates the sorting of microRNA-30c-5p into large extracellular vesicles. J. Extracell. Vesicles *9*, 1786967.

iScience, Volume *24*

Supplemental information

Small extracellular vesicles with LncRNA H19 “overload”: YAP Regulation as a Tendon Repair Therapeutic Tactic

Shi-Cong Tao, Ji-Yan Huang, Zi-Xiang Li, Shi Zhan, and Shang-Chun Guo

Table S1. Sequencing primers for H4535 (pLenti-EF1a-EGFP-F2A-Puro-CMV-H19) (Related to Figure 7)

Types of primers	Label	Sequence
Forward sequencing primers	CMV-F	CGCAAATGGGCGGTAGGCGTG
Reverse sequencing primers	WPRE-R	CATAGCGTAAAAGGAGCAACA

Table S2. Sequencing results of H4535 (Related to Figure 7)

H4535 Sequencing
NNNNNTNNNGNNNATTTCAAAAATGTCGTAACAACTCCGCCCCATTGACGCAAATGGGCGGTAGGCGTGTACGGTGGGAGNTCTATATAA GCAGAGCTCGTTTAGTGAACCGTCAGATCGAATTCAGTTAGAAAAAGCCCGGGCTAGGACCGAGGAGCAGGGTGAGGGAGGGGGTGGGAT GGGTGGGGGGTAACGGGGGAAACTGGGGAAGTGGGGAACCGAGGGGCAACCAGGGGAAGATGGGGTGCTGGAGGAGAGCTTGTGGGAGCC AAGGAGCACCTTGGACATCTGGAGTCTGGCAGGAGTGATGACGGGTGGAGGGGCTAGCTCGAGGCAGGGCTGGTGGGGCCTGAGGCCAGT GAGGAGTGTGGAGTAGGCGCCCAGGCATCGTGCAGACAGGGCGACATCAGCTGGGGACGATGGGCCTGAGCTAGGGCTGGAAAGAAGGGG GAGCCAGGCATTCATCCCGGTCACTTTTGGTTACAGGACGTGGCAGCTGGTTGGACGAGGGGAGCTGGTGGGCAGGGTTTGATCCCAGGG CCTGGGCAACGGAGGTGTAGCTGGCAGCAGCGGGCAGGTGAGGACCCCATCTGCCGGGCAGGTGAGTCCCTTCCCTCCCCAGGCCTCGCT TCCCCAGCCTTCTGAAAGAAGGAGGTTTAGGGGATCGAGGGCTGGCGGGGAGAAGCAGACACCCTCCCAGCAGAGGGGCAGGATGGGGGC AGGAGAGTTAGCAAAGGTGACATCTTCTCGGGGGGAGCCGAGACTGCGCAAGGCTGGGGGGTTATGGGCCCGTTCCAGGCAGAAAGAGCA AGAGGGCAGGGAGGGAGCACAGGGGTGGCCAGCGTAGGGTCCAGCACGTGGGGTGGTACCCCAGGCCTGGGTCAGACAGGGACATGGCAG GGGACACAGGACAGAGGGGTCCCCAGCTGCCACCTCACCCACCGCAATTCATTTAGTAGCAGGCACAGGGGCAGCTCCGGCACGGCTTTC TCAGGCCTATGCCGGAGCCTCGAGGGCTGGAGAGCGGGAAGACAGGCAGTGCTCGGGGAGTTGCAGCAGGACGTCACCAGGAGGGCGAAG CGGCCACGGGAGGGGGGCCCCGGGACATTGCGCAGCAAGGAGGCTGCAGGGGCTCGGCCTGCGGGCGCCGGTCCCACGAGGCACTGCGGC CCAGGGTCTGGTGCGGAGAGGGCCCACAGTGGACTTGGTGACGCTGTATGCCCTCACCGCTCAGCCCCTGGGGCTGGCTTGGCAGACAGT ACAGCATCCAGGGGAGTCAAGGGCATGGGGCGAGACCAGACTAGGCGAGGCGGGCGGGGCGGAGTGAATGAGCTCTCAGGAGGGAGGATG GTGCAGGCAGGGGTGAGGAGCGCAGCGGGCGGCGAGCGGGAGGCACTGGCCTCCAGAGCCCGTGGCCAAGGCGGGCCTCGCGGGCGGCGA CGGAGCCGGGATCGGTGCCTCAGCGTTCGGGCTGGAGACGAGGCCAGGTCTCCAGCTGGGGTGGACGTGCCCACCAGCTGCCGAAGGCCA AGACGCCAGGTCCGGTGGACGTGACAAGCAGGACATGACATGGTCCGGTGTGACGGCGAGGACAGAGGAGGCGCGTCCGGCCTTCCTGAA CACCTTAGGCTGGTGGGGCTGCGGCAAGAAGCGGGTCTGTTTCTTTACTTCCTCCACGGAGTCGGCACACTATGGCTGCCCTCTGGGCTC CCAGAACCCACAACATGAAAGAAATGGTGCTACCCAGCTCAAGCCTGGGCCTTTGAATCCGGACACAAAACCCTCTAGCTTGGAAATGAA TATGCTGCACTTTACAACCACTGCACTACCTGACTCAGGAATCGGCTCTGGAAGGTGAAGCTAGAGGAACCAGACCTCATCAGCCCAACA TCAAAGACACCATCGGAACAGCAGCGCCCGCAGCACCCACCCCGCACCGGCGACTCCATCTTCATGGCCACCCCCTGCGGCGGACGGTTG ACCACCAGCCACCACATCATCCCAGAGCTGAGCTCCTCCAGCGGGATGACGCCGTCCCCACCACCTCCCTCTTCTTCTTTTTCATCCTTC TGTCTCTTTGTTTCTGAGCTTTCCTGTCTTTCCTTTTTTCTGAGAGATTCAAAGCCTCCACGACTCTGTTTCCCCCGTCCCTTCTGAATT TAATTTGCACTAAGTCATTTGCACTGGTTGGAGTTGTGGAGACGGCCTTGAGTCTCAGTACGAGTGTGCGTGAGTGTGAGCCACCTTGGC AAGTGCCTGTGCAGGGCCCGGCCGCCCTCCATCTGGGCCGGGTGACTGGGCGCCGGCTGTGTGCCCGAGGCCTCACCCTGCCCTCGCCTA GTCTGGAAGCTCCGACCGACATCACGGAGCAGCCTTCAAGCATTCCATTACGCCCCATCTCGCTCTGTGCCCCTCCCCACCAGGGCTTCA GCAGGAGCCCTGGACTCATCATCAATAAACACTGTTACAGCAAGGATCCTCAACCTCTGGATTACAAAATTTGTGAAAGATTGACTGGTA TTCTTAACTATGTTGCTCCTTTACGCTATGTGGATACGCTGCTTTAANGNNNNNNNNN

Table S3. Alignment between NR_002196 (H19, transcript variant 1) and H4535 (Related to Figure 7)

Alignment between H4535 and NR_00219

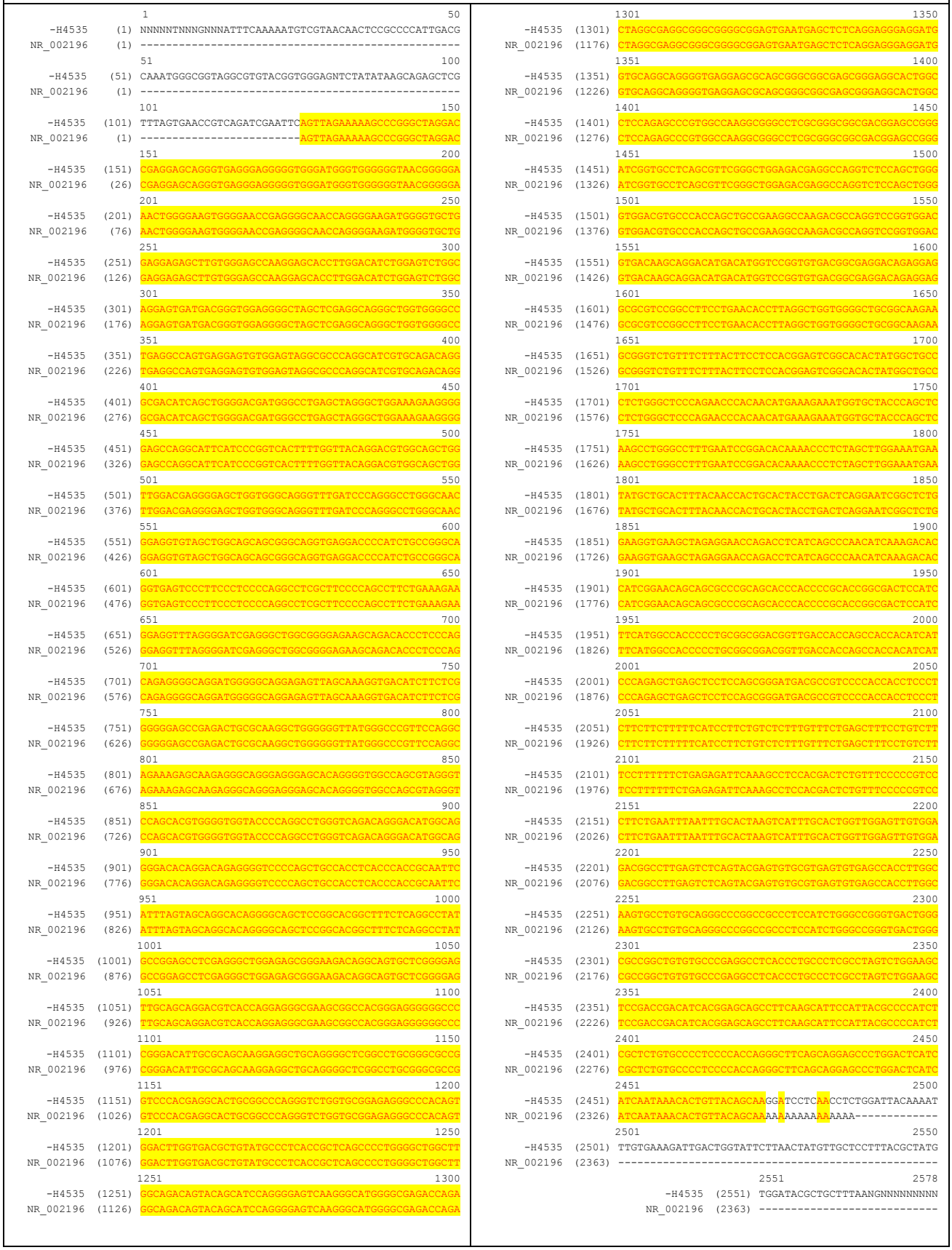

Table S4. PCR primers used in this study (Related to Figure 2, 3, 4 and 7)

Gene	Forward primer	Reverse primer
H19	AAAGCCTCCACGACTCTGTT	GCTCACACTCACGCACACTC
SCX	CGAGAACACCCAGCCCAAAC	CTGCGAATCGCTGTCTTTCTGTC
TNMD	TGGGTGGTCCCTCAAGTGAAAGT	CTCGACGGCAGTAAATACAACAATA
CYR61	AAGGAGCTGGGATTCGATGC	CATTCCAAAAACAGGGAGCCG
CTGF	TGTGCACCGCCAAAGATGG	ACGTGCACTGGTACTTGCAG
ANKRD1	AGCCCAGATCGAATTCCGTG	TGAGCAACTTATCTCGGGCG
GAPDH	GGGAAGGTGAAGGTCGGAGT	GGGGTCATTGATGGCAACA

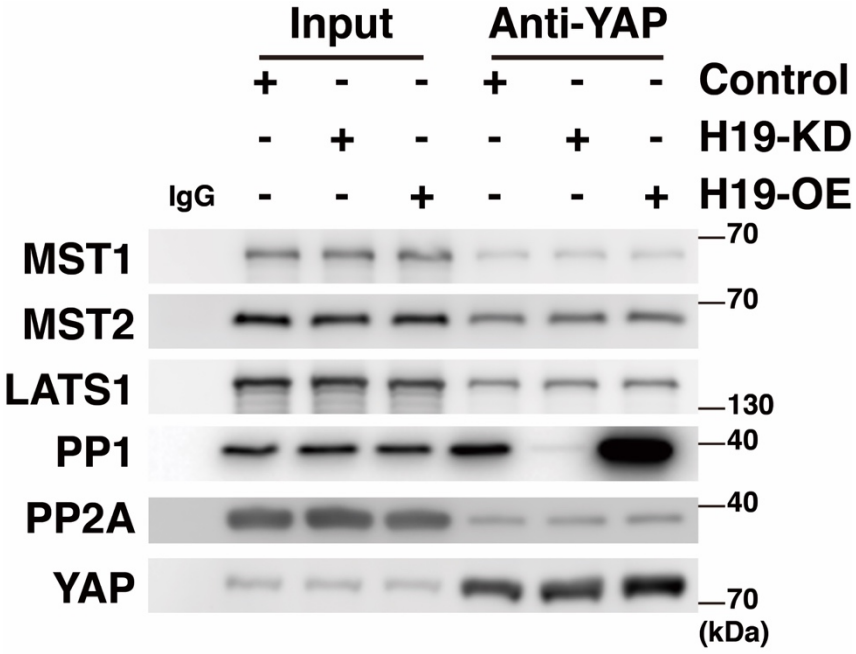

Figure S1. The effect of H19 on the interaction between YAP and MST1/MST2/LATS1/PP1/PP2A. The interaction between YAP and MST1/MST2/LATS1/PP1/PP2A were measured by immunoprecipitation and western blot analyses after overexpression or knockdown of H19. (Related to Figure 4)

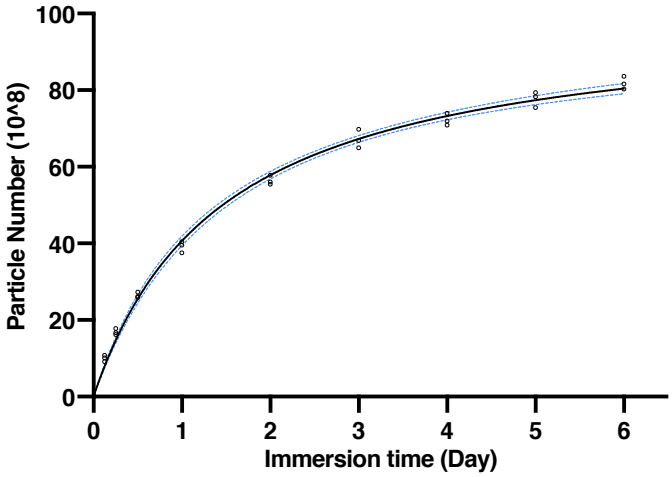

Figure S2. Release curve of sEVs. The hollow circles represented the data point. The blue dotted lines showed the 95% confidence interval. (Related to Figure 8)

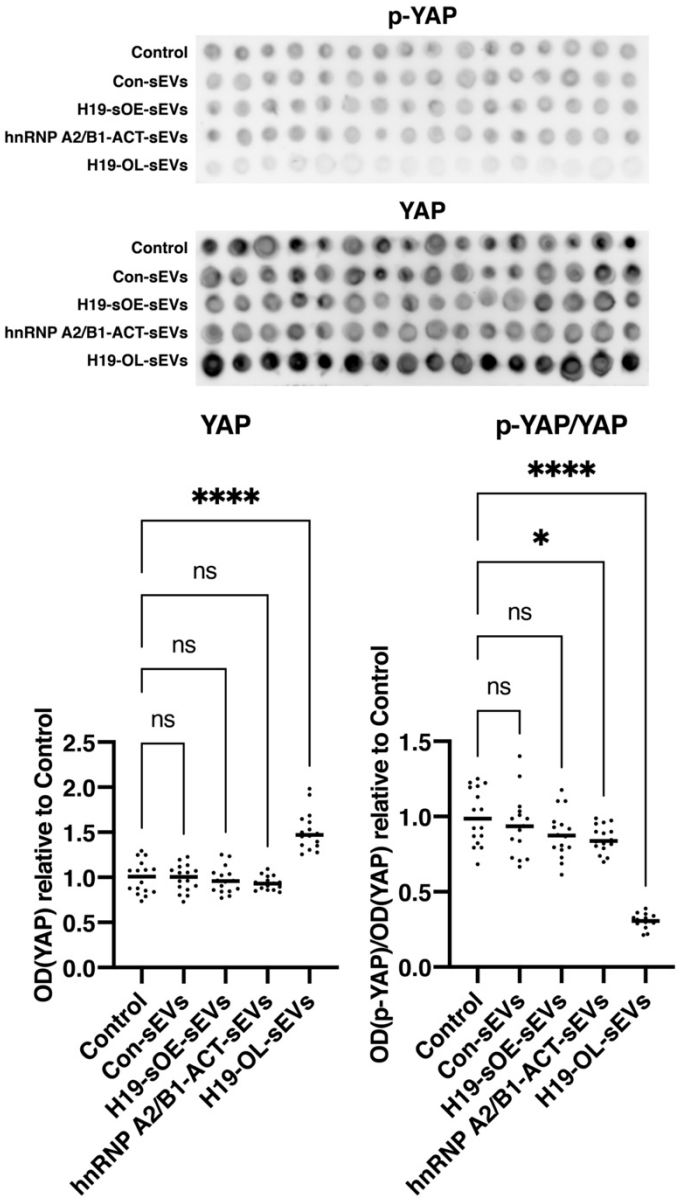

Figure S3. Dephosphorylation and accumulation of YAP in regenerated tendon tissue. Data are presented as mean ± standard deviation. Significant differences (one-way ANOVA test): ns, no significant difference ($p > 0.05$); *, $p < 0.05$; **, $p < 0.01$; ***, $p < 0.001$; ****, $p < 0.0001$. (Related to Figure 8)

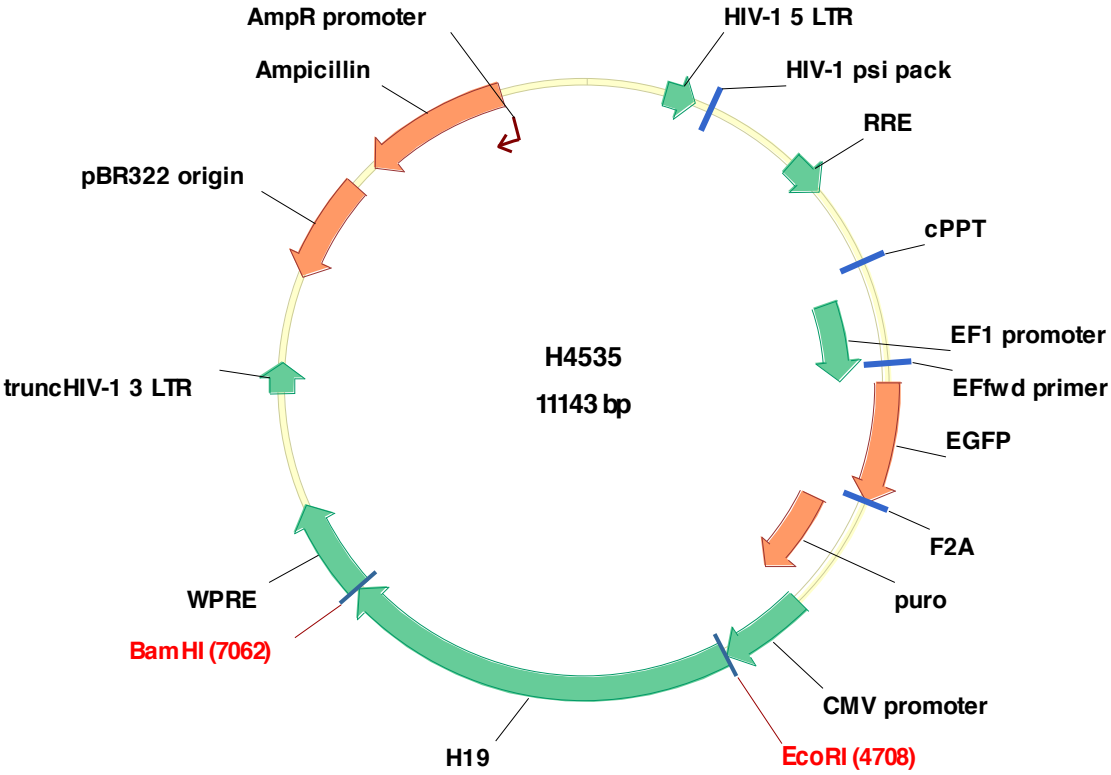

Figure S4. Plasmid structure of H4535 (pLenti-EF1a-EGFP-F2A-Puro-CMV-H19). (Related to Figure 7)

Transparent Methods

1. Ethics statement

The tendon tissues from donors (male, 25~32 years old without systemic disease, amputation because of severe trauma) were collected in our institution/hospital, with permission and the written informed consent of the patients and approval from the Ethical Committee of Shanghai Sixth People's Hospital, Shanghai Jiao Tong University School of Medicine. Sprague-Dawley rats (male, four months old) were purchased from the Shanghai Laboratory Animal Company (Shanghai, China) and were fed in a specific pathogen-free environment. A good standard of animal welfare was provided for all the experimental animals, and the experimental methods were approved by the Animal Research Ethics Committee of Shanghai Jiao Tong University Affiliated Sixth People's Hospital, Shanghai Jiao Tong University School of Medicine. All procedures were conducted following the Declaration of Helsinki and standard guidelines.

2. Isolation and identification of human TSPCs

TSPCs were isolated from tendon tissues discarded during amputation operations and cultured as previously described(Bi et al., 2007). In brief, after stripping off the tendon sheath and surrounding paratenon, the tendon tissues were cut into small pieces, before being digested for 1 hour at 37 °C with 3 mg/mL Type I collagenase (Gibco™, Thermo Fisher Scientific, Waltham, MA, USA) and 4 mg/ml Dispase II (Gibco™, Thermo Fisher Scientific). Single-cell suspensions were cultured in Minimum Essential Medium alpha (α-MEM; Gibco™, Thermo Fisher Scientific), supplemented with 10% fetal bovine serum (FBS; Gibco™, Thermo Fisher Scientific).

The specific cell surface antigen markers of TSPCs were examined via flow cytometry (FCM) using a CytoFLEX Flow Cytometer (Beckman Coulter, Indianapolis, IN, USA) and analysed using CytExpert software (Beckman Coulter). The primary antibodies, including anti-CD73-PE, anti-CD90-PE, anti-CD44-PE, anti-CD34-PE, anti-CD45-PE, and anti-CD105-FITC, were purchased from BD Pharmingen (San Jose, CA, USA).

A trilineage-induced differentiation assay was also performed to identify the adipogenic, osteogenic, and chondrogenic differentiation potential of TSPCs. In brief, osteogenic differentiation was induced by replacing the complete culture medium with StemPro™ Osteogenesis Differentiation Kit (Gibco™, Thermo Fisher Scientific) and culturing for 3 weeks. For adipogenic differentiation, the StemPro™ Adipogenesis Differentiation Kit (Gibco™, Thermo Fisher Scientific) was used for 2 weeks. For

chondrogenic induction, cells were encapsulated in alginate gel beads and cultured using a StemPro™ Chondrogenesis Differentiation Kit (Gibco™, Thermo Fisher Scientific) for 4 weeks. The specific procedures of inducing differentiation were described in the instruction book provided by manufacturer.

3. Regulation of gene expression and isolation of sEVs

HnRNP A2/B1-ACT plasmid (sc-400635-ACT), control CRISPR activation plasmid (sc-437275), YAP-KO (sc-400040), PP1α-ACT (sc-400318-ACT), and PP1α-KO (sc-400318) were purchased from Santa Cruz Biotechnology (Santa Cruz, CA, USA). These are commercially-available, ready-to-use plasmids, which were used according to the manufacturer's protocol.

pCMV-flag S127A YAP (S127A plasmid) was a gift from Kunliang Guan (Addgene plasmid # 27370; http://n2t.net/addgene:27370; RRID:Addgene_27370)(Zhao et al., 2007). pcDNa3.1(+)_A009-H19 (H19-OE plasmid) was a gift from Alexandra Kiemer (Addgene plasmid # 122473; http://n2t.net/addgene:122473; RRID:Addgene_122473)(Schultheiss et al., 2017). Their detailed sequences can be found on the Addgene website (https://www.addgene.org/). In order to establish cells stably over-expressing H19 (H19-sOE) for the "manufacture" of H19-containing sEVs, we further constructed a lentivirus vector H4535 (pLenti-EF1a-EGFP-F2A-Puro-CMV-H19) with help from Obio Technology (Shanghai, China). The sequencing primers (Table S1), sequencing results (Table S2), sequence alignment (Table S3), and plasmid structure (Figure S4) are shown in Supplementary materials. H19 stably over-expressing TSPCs (H19-sOE-TSPCs), hnRNP A2/B1-activated TSPCs (hnRNP A2/B1-ACT-TSPCs), and TSPCs co-overexpressing H19 and its "chaperone" hnRNP A2/B1 (H19-CP-TSPCs) were prepared.

In addition, LncRNA-H19 Smart Silencer (H19-KD) was purchased from RiboBio (Guangzhou, China), and transfection was performed according to the manufacturer's protocol. Verteporfin (a small molecule chemical drug to disrupt the YAP–TEAD interaction) was used for the observation of biological functions and effects of YAP activation(Tao et al., 2017c).

4. Isolation and identification of sEVs

Conditioned medium (CM) was collected, and sEVs were isolated as described by Tao et al.(Tao et al., 2017a; Tao et al., 2017c). In brief, after removing dead cells and cellular debris (300 × g for 15 minutes and then 2,000 × g for 15 minutes), the supernatants were filtered through a 0.22 μm filter (Merck, Merck KGaA, Darmstadt, Germany) to further remove residual cellular debris. The filtered solution was added into the upper compartment of a 15-ml Amicon Ultra-15 Centrifugal Filter Unit (Merck),

and centrifuged at 4,000 × g until the upper compartment was concentrated to approximately 200 μL. The ultrafiltration liquid was washed with Dulbecco's phosphate-buffered saline (DPBS, Gibco™, Thermo Fisher Scientific), and ultrafiltration was repeated three times. The liquid was then ultracentrifuged using a sterile Ultra-Clear tube (Beckman Coulter) with a 30% sucrose-D_2O cushion at 100,000 × g for 1 hour. The pellets were then resuspended in 200 μL of DPBS. All procedures were performed at 4°C. Hence, Con-sEVs (derived from TSPCs), H19-sOE-sEVs (derived from H19-sOE-TSPCs), hnRNP A2/B1-ACT-sEVs (from hnRNP A2/B1-ACT-TSPCs), and H19-OL-sEVs (from H19-CP-TSPCs; both H19-sOE and hnRNP A2/B1-ACT; H19 "overloading") were prepared for subsequent experiments.

sEVs were identified according to their size distribution, morphologies, and specific surface markers including CD9, CD63, and CD81, as used in our previous studies(Guo et al., 2016; Guo et al., 2017; Tao et al., 2017a; Tao et al., 2017b; Tao et al., 2017c). In brief, morphologies of sEVs were observed using transmission electron microscopy (TEM). The size distribution of sEVs was measured by using Nanosizer technology (Malvern Instruments, Malvern, United Kingdom). Expression of the specific surface markers were analyzed by Western blot (WB).

5. Sodium alginate hydrogel preparation

The different groups of isolated sEVs were first diluted to 10×10^{11}/mL as a stock solution (for the control group, the stock solution was replaced by the same volume of deionized water). Sodium alginate hydrogel was prepared based on the method mentioned in our previous research(Guo et al., 2017). In brief, after dry sodium alginate powder (2% w/v) was mixed in deionized water and agitated for one hour for complete dissolution, the subsequent operations took place on ice, as low temperature polymerization is beneficial to maintaining the biological activity of sEVs(Tao et al., 2017a). The stock solution (10% v/v) was mixed into this system under gentle agitation. Next, the mixture was poured into 10 cm culture dishes (Corning, NY, USA) filled with calcium chloride ($CaCl_2$) solution (5% w/v), gelatinized at 4°C overnight, and redundant $CaCl_2$ solution was discarded. The final concentration of sEVs in each group in the sodium alginate hydrogel was 10^{11}/mL. Finally, the gelatinized gels (~2 mm height) were carefully cut into 0.5 cm (width) × 1 cm (length) blocks.

6. Release curve of sEVs

Based on our previous research(Tao et al., 2017a), sodium alginate hydrogel blocks loaded with sEVs were immersed in MesenGro® hMSC medium (StemRD, Burlingame, CA, USA) for 3, 6, or 12 hours

or 1, 2, 3, 4, 5, or 6 days. Quantification of sEVs was performed using a CD63 ExoELISA kit (System Biosciences, Palo Alto, CA, USA) according to the instructions provided by the manufacturer.

7. YAP localisation

Following the method described in our previous reports(Guo et al., 2016; Guo et al., 2017; Tao et al., 2016), TSPCs were seeded into a confocal glass-bottomed 35 mm dish with 20 mm micro-well cover glass (Solarbio, Beijing, China). After incubating with Con-sEVs (10^9/mL), H19-sOE-sEVs (10^9/mL), hnRNP A2/B1-ACT-sEVs (10^9/mL), or H19-OL-sEVs (10^9/mL), YAP localisation was examined. Cells were incubated with a rabbit anti-human YAP antibody (Cell Signalling Technology, CST; Danvers, MA, USA) for 2 h and Alexa Fluor®488-conjugated secondary antibody (CST) for 1 h at 25°C. Isotype control antibodies (CST) were used as negative controls. Nuclei were stained with 4, 6-diamidino-2-phenylindole (DAPI; 0.5 μg/mL; Invitrogen™, Thermo Fisher Scientific) for 5 min. Cells were analysed using a confocal microscope (Zeiss LSM720, Zeiss Microscopy GmbH, Jena, Germany).

8. Cell proliferation and migration assays

Cells seeded into 6-well plates (Corning) were treated with empty vector, H19-KD, H19-OE, H19-KD+S127A, H19-OE+YAP-KO, H19-OE+verteporfin, H19-KD+PP1α-ACT, or H19-OE+PP1α-KO, or with Con-sEVs, H19-sOE-sEVs, hnRNP A1/B2-ACT-sEVs, or H19-OL-sEVs, and follow-up experiments were carried out 48 hours later.

For proliferation assays, 2×10^4 cells/well were re-seeded into 48-well plates, and then stained using a Cell-Light EdU Apollo488 kit (RiboBio, Guangzhou, China) to examine cell proliferation as previously reported(Tao et al., 2017b). In brief, EdU working solution (0.15 μL EdU + 150 μL complete culture medium) was added into each well and incubated at 37 °C for 3 hours. Then, cells were then digested using trypsin-EDTA (Gibco™, Thermo Fisher Scientific), washed using DPBS, fixed in 4% paraformaldehyde (PFA; Wuhan Servicebio Technology, Wuhan, China) for 15 minutes, neutralized with 2 mg/mL glycine (Solarbio) and washed three times in DPBS before permeabilising with 0.4% Triton X-100 (Solarbio) for 5 minutes and finally washing three times with DPBS. Cells were resuspended and incubated for 10 minutes using the Apollo staining solution (in the kit). After washed twice in 0.4% Triton X-100, cells were resuspended in DPBS. FCM was carried out using a CytoFLEX Flow Cytometer (Beckman Coulter) and analysed using the CytExpert software (Beckman Coulter).

For migration assays, approximately 5×10^4 cells/well from each group were re-seeded into the

upper chambers of a 24-well 8-μm transwell plate (Corning). After incubation for 6 hours, cells were fixed with 4% PFA for 5 minutes and then stained for 5 minutes with 0.5% crystal violet (Solarbio). The upper chambers were washed three times in DPBS, and then the cells on the upper surface were carefully removed with a cotton swab. Five fields per well (selected randomly) were photographed using a Nikon ECLIPSE Ts2R microscope (Nikon Corporation, Japan) and assessed by two pathologists in a blinded manner.

9. Collagen deposition assay

Sirius red staining assay was performed as previously reported(Chhana et al., 2014; Huang et al., 2013), to estimate collagen deposition. Briefly, after treatment with empty vector or H19-KD, H19-OE, H19-KD+S127A, H19-OE+YAP-KO, H19-OE+verteporfin, H19-KD+PP1α-ACT, H19-OE+PP1α-KO, or with Con-sEVs, H19-sOE-sEVs, hnRNP A1/B2-ACT-sEVs, and H19-OL-sEVs, cells were seeded into a 6-well plate at 5×10^5 cells/mL and incubated with complete α-MEM in the presence of 10 ng/mL TGF-β1 (PeproTech, Rocky Hill, NJ, USA)(Zhang et al., 2018a). According to the manufacturer's protocol, the cells were stained with a Picrosirius red solution kit purchased from Solarbio. The culture plates after staining were photographed using a DSC-RX1 professional compact camera with 35 mm full-frame sensor (Sony, Japan).

10. Reverse transcription-polymerase chain reaction (RT-PCR) and polyacrylamide gel electrophoresis (PAGE)

Total RNA was extracted from cells with TRIzol Reagent (Invitrogen™, Thermo Fisher Scientific), while total RNA and protein was extracted from sEVs with a Total Exosome RNA & Protein Isolation Kit (Invitrogen™, Thermo Fisher Scientific) referring to the manufacturer's protocol. RT-PCR was performed using QIAGEN OneStep Ahead RT-PCR Kit (Qiagen, Frederick, MD, USA). In brief, after preparing the master mixes (for each reaction, 10 μL 5× QIAGEN OneStep RT-PCR Buffer, 2 μL dNTP Mix, 2 μL QIAGEN OneStep RT-PCR Enzyme Mix, 2 μL forward primers, 2 μL reverse primers and 30 μL RNase-free water), 2 μL template RNA was mixed with 48 μL mater mixes in individual PCR tubes (Solarbio). The thermal cycler was programmed according to according to the instructions provided by the manufacturer. PCR products were mixed a ratio of 1:5 with 6× DNA Loading Buffer (Solarbio), added into the wells of precast PAGE gels (Solarbio) and electrophoresed at 150 V for 40 minutes. The gels, after electrophoresis, were immersed in SYBR Green I (Solarbio) working

solution and then photographed using the ultraviolet (UV) fluorescence mode of FluorChem Systems (ProteinSimple, San Jose, CA, USA). The primer sequences are shown in Table S4.

11. WB analysis and antibodies

WB analysis was performed as reported previously(Guo et al., 2017; Tao et al., 2017a; Tao et al., 2017b), after protein lysate preparation. In brief, protein lysates of cells or sEVs were mixed a ratio of 1:4 with 5× sodium dodecyl sulfate (SDS)-PAGE loading buffer (Solarbio) and heated at 95°C for 5 minutes. Samples were separated by 10% SDS-PAGE gels, prepared by PAGE Gel Fast Preparation Kit (EpiZyme Biotech, Shanghai, China), at 120 V for 1 hour, and blotted onto a polyvinylidene di-fluoride (PVDF) membrane (Merck) for 90 minutes at 200 mA. After blocking, primary antibodies incubation and secondary antibodies incubation, the immunoreactive bands were visualized using Omni-ECL™ Femto Light Chemiluminescence Kit (EpiZyme Biotech) and imaged using the chemiluminescence mode of FluorChem Systems (ProteinSimple).

The primary antibodies used were as follows: anti-CD9, anti-CD63, anti-CD81 (System Biosciences); anti-SCXA (SCX), anti-tenomodulin (TNMD) and anti-hnRNP A2/B1 (Abcam, Cambridge, UK); anti-YAP and phosphorylated YAP (p-YAP), anti-LAST1 and phosphorylated LAST1 (p-LAST1), anti-MST1, anti-MST2, anti-p-MST1/2, anti-GAPDH, anti-HistoneH3, anti-HA-Tag (CST); anti-PP1 (R&D Systems, Minneapolis, MN, USA); anti-PP2A (Novus Biologicals, Littleton, CO, USA).

12. RNA pull-down assays

RNA pull-down assays were performed according to the manufacturer's instructions. Briefly, biotin-labelled *H19* RNAs were first transcribed *in vitro* using the biotin RNA labelling mix (Roche, Basel, Switzerland) and the MEGAscript T7 Transcription Kit (AM1334, Thermo Fisher Scientific). Biotinylated RNAs were mixed with streptavidin agarose beads using the Pierce Magnetic RNA–Protein Pull-Down Kit (20,164, Thermo Fisher Scientific) and then the RNA-captured beads were washed. After total cell lysates were freshly prepared and incubated with RNA-captured beads at 4°C rotating overnight, the RBP complex was washed and eluted. Finally, the eluted protein was boiled and subjected to WB analysis.

13. RNA immunoprecipitation (RIP) assays

The protein/RNA binding to YAP protein was verified and conducted according to the instructions provided with the Magna RIP™ RNA-Binding Protein Immunoprecipitation Kit (Merck). TSPCs were

placed in an ice bath with RIP Lysis Buffer. Bead-antibody complexes were prepared according to the instructions. Part of the cell lysate was used as the input, and the rest was incubated with magnetic bead–antibody complexes. Samples were then placed on a magnetic base, to collect the magnetic bead–antibody–protein–RNA complexes, after washing with RIP wash buffer three times. RNAs in the samples and the input were separately extracted for subsequent PCR and PAGE, while proteins were separately extracted for subsequent WB assays.

14. Database usage and visualization

The expression of H19 in different healthy tissues was analysed in the Genotype-Tissue Expression (GTEx) database by browsing and by searching all data for the H19 gene. To further investigate the role of H19 in TSPCs, we predicted H19 co-expression using the RNA–RNA CoExpression module/tool of the ENCORI database (The Encyclopaedia of RNA Interactomes(Fan et al., 2020), previously called starBase(Li et al., 2014)). GeneMANIA (http://www.genemania.org), a database for visualisation of gene interactions(Warde-Farley et al., 2010), was used to visualise the known evidence of interaction between genes, by importing the gene of interest.

15. Preparation of the rat patellar tendon defect model and experimental groups

The study included ninety-six four-month-old male Sprague-Dawley rats weighing between 250–330 g each. All animal procedures were conducted with the approval of the Institutional Committee on the Care and Use of Animals of Shanghai Jiao Tong University Affiliated Sixth People's Hospital (Shanghai, China). Before experimentation, the animals were fed standard rat chow and water, and housed in cages with a controlled temperature and a 12-h light/dark cycle.

The animals were randomly assigned to six groups (sixteen rats per group), each based on the treatment they received after surgery: (G1), normal group (sham surgery); (G2) control group; (G3), Con-sEVs group; (G4), H19-sOE-sEVs group; (G5), hnRNP A2/B1-sEVs group; (G6), H19-OL-sEVs group.

To establish the rat tendon defect model, according to a well-recognized protocol(Ni et al., 2013; Yu et al., 2020), the central one-third of the left knee patellar tendon (1 mm in width) was removed using two stacked sharp blades (in height: from the distal apex of the patella to the insertion of the tibia tuberosity). Then, different preparations of prefabricated hydrogels were used to cover the defect.

16. Histological analysis

The rats were allowed to move freely in their cages until sacrificed. None of the rats died before the

scheduled sacrifice. Four weeks after the surgery, all the rats in each group were sacrificed, and tendon samples were harvested for biomechanical testing from eight of the rats, while the other eight rats in each group were used for histological examination.

The pre-treatment of the tendon tissue obtained was performed according to the method described in previous studies(Ni et al., 2012; Ni et al., 2013; Wu et al., 2016; Yin et al., 2016; Yu et al., 2020; Zhang et al., 2018b). First, the patellar tendon–tibia composite was isolated and removed together with the surrounding muscles. Next, the lateral and medial healthy tissue was removed using two stacked blades with a 0.6 mm interval. After this step, almost half the regenerated tissue still remained. The remaining regenerated tissue was carefully removed from the vicinity of the normal tissue with a blade, and protein was extracted using a ZK-III-F high-speed low-temperature tissue homogenizer (Wuhan Servicebio Technology) after snap-freezing in liquid nitrogen. As a widely accepted, simple and convenient method(Lee and Lemmon, 2001; RENART et al., 1996), dot blot was used to measure the phosphorylation level of YAP. Briefly, after protein quantification using Pierce™ Rapid Gold BCA Protein Assay Kit (Thermo Fisher Scientific), the protein concentration was diluted to 1μg/μL, and then 1 μL of samples were spotted onto nitrocellulose membranes (Solarbio). After membrane drying, subsequent steps were similar to western blot.

For subsequent biomechanical experiments, the processed tissue consisted of only the regenerated tissue in the window-shaped wound together with the connection to its bony ends.

For subsequent histological examination, the bony ends were carefully removed, and the tendon specimens were fixed in formalin, embedded and sectioned for histological analysis. The tissue sections were stained with haematoxylin and eosin (H&E), Masson's trichrome, Safranin O & Fast green, and Sirius Red. The sections were observed under a light microscope (LEICA DM 4000 B, Germany). Polarised light was used for the assessment of collagen fibre alignment after Sirius Red staining. The study personnel were blinded to the experimental treatments.

17. Biomechanical testing

The healing tendon tissues of eight rats in each group 4 weeks post-surgery were used for biomechanical tests following the previously-established protocol(Ni et al., 2012; Ni et al., 2013; Wu et al., 2016; Yin et al., 2016; Yu et al., 2020; Zhang et al., 2018b). A VisualSonics Vevo 770® High-Resolution Imaging System (Visualsonics, Toronto, Canada) was used to measure the cross-sectional area. All tendons were placed in saline at room temperature for 1 hour before mechanical tests. All

mechanical tests were performed using the Instron 5569 biomechanical test system (Instron, Boston, MA, USA).

The test to failure was performed at a testing speed of 40 mm/min, a preload of 0.1 N using a 50-N load cell and conducted with a cyclic elongation of 0–0.5 mm cycles at 5 mm/min. The load-displacement curve of the healing tendon tissue was recorded. The stress at failure (N/mm^2) was calculated based on the ultimate load divided by the cross-sectional area at the breaking point. The Young's modulus (N/mm^2) was calculated according to the linear slope of a stress–strain curve.

18. Statistical analysis

Statistical analysis was performed using SPSS 21.0 software (IBM, Armonk, NY, USA). Data are presented as mean ± standard deviation. Differences between groups were analysed using one-way analysis of variance (one-way ANOVA test). Statistical significance was indicated when $p < 0.05$.

References

Bi, Y., Ehirchiou, D., Kilts, T.M., Inkson, C.A., Embree, M.C., Sonoyama, W., Li, L., Leet, A.I., Seo, B.M., Zhang, L., *et al.* (2007). Identification of tendon stem/progenitor cells and the role of the extracellular matrix in their niche. Nature medicine *13*, 1219-1227.

Chhana, A., Callon, K.E., Dray, M., Pool, B., Naot, D., Gamble, G.D., Coleman, B., McCarthy, G., McQueen, F.M., Cornish, J., *et al.* (2014). Interactions between tenocytes and monosodium urate monohydrate crystals: implications for tendon involvement in gout. Annals of the rheumatic diseases *73*, 1737-1741.

Fan, K., Zebisch, A., Horny, K., Schrama, D., and Becker, J.C. (2020). Highly Expressed miR-375 is not an Intracellular Oncogene in Merkel Cell Polyomavirus-Associated Merkel Cell Carcinoma. Cancers *12*.

Guo, S.C., Tao, S.C., Yin, W.J., Qi, X., Sheng, J.G., and Zhang, C.Q. (2016). Exosomes from Human Synovial-Derived Mesenchymal Stem Cells Prevent Glucocorticoid-Induced Osteonecrosis of the Femoral Head in the Rat. International journal of biological sciences *12*, 1262-1272.

Guo, S.C., Tao, S.C., Yin, W.J., Qi, X., Yuan, T., and Zhang, C.Q. (2017). Exosomes derived from platelet-rich plasma promote the re-epithelization of chronic cutaneous wounds via activation of YAP in a diabetic rat model. Theranostics *7*, 81-96.

Huang, Y., de Boer, W.B., Adams, L.A., MacQuillan, G., Rossi, E., Rigby, P., Raftopoulos, S.C., Bulsara, M., and Jeffrey, G.P. (2013). Image analysis of liver collagen using sirius red is more accurate and correlates better with serum fibrosis markers than trichrome. Liver international : official journal of the International Association for the Study of the Liver *33*, 1249-1256.

Lee, A., and Lemmon, M.A. (2001). Analysis of phosphoinositide binding by pleckstrin homology domain from dynamin. Methods in enzymology *329*, 457.

Li, J.H., Liu, S., Zhou, H., Qu, L.H., and Yang, J.H. (2014). starBase v2.0: decoding miRNA-ceRNA, miRNA-ncRNA and protein-RNA interaction networks from large-scale CLIP-Seq data. Nucleic acids research *42*, D92-97.

Ni, M., Lui, P.P., Rui, Y.F., Lee, Y.W., Lee, Y.W., Tan, Q., Wong, Y.M., Kong, S.K., Lau, P.M., Li, G., *et al.* (2012). Tendon-derived stem cells (TDSCs) promote tendon repair in a rat patellar tendon window defect model. Journal of orthopaedic research : official publication of the Orthopaedic Research Society *30*, 613-619.

Ni, M., Rui, Y.F., Tan, Q., Liu, Y., Xu, L.L., Chan, K.M., Wang, Y., and Li, G. (2013). Engineered scaffold-free tendon tissue produced by tendon-derived stem cells. Biomaterials *34*, 2024-2037.

RENART, J., BEHRENS, M.M., FERNÁNDEZ-RENART, M., and MARTINEZ, J.L. (1996). Immunoblotting techniques. In Immunoassay (Elsevier), pp. 537-554.

Schultheiss, C.S., Laggai, S., Czepukojc, B., Hussein, U.K., List, M., Barghash, A., Tierling, S., Hosseini, K., Golob-Schwarzl, N., Pokorny, J., *et al.* (2017). The long non-coding RNA H19 suppresses carcinogenesis and chemoresistance in hepatocellular carcinoma. Cell Stress *1*, 37-54.

Tao, S.C., Gao, Y.S., Zhu, H.Y., Yin, J.H., Chen, Y.X., Zhang, Y.L., Guo, S.C., and Zhang, C.Q. (2016). Decreased extracellular pH inhibits osteogenesis through proton-sensing GPR4-mediated suppression of yes-associated protein. Scientific reports *6*, 26835.

Tao, S.C., Guo, S.C., Li, M., Ke, Q.F., Guo, Y.P., and Zhang, C.Q. (2017a). Chitosan Wound Dressings Incorporating Exosomes Derived from MicroRNA-126-Overexpressing Synovium Mesenchymal Stem Cells Provide Sustained Release of Exosomes and Heal Full-Thickness Skin Defects in a Diabetic Rat Model. Stem cells translational medicine *6*, 736-747.

Tao, S.C., Yuan, T., Rui, B.Y., Zhu, Z.Z., Guo, S.C., and Zhang, C.Q. (2017b). Exosomes derived from human platelet-rich plasma prevent apoptosis induced by glucocorticoid-associated endoplasmic reticulum stress in rat osteonecrosis of the femoral head via the Akt/Bad/Bcl-2 signal pathway. Theranostics *7*, 733-750.

Tao, S.C., Yuan, T., Zhang, Y.L., Yin, W.J., Guo, S.C., and Zhang, C.Q. (2017c). Exosomes derived from miR-140-5p-overexpressing human synovial mesenchymal stem cells enhance cartilage tissue regeneration and prevent osteoarthritis of the knee in a rat model. Theranostics *7*, 180-195.

Warde-Farley, D., Donaldson, S.L., Comes, O., Zuberi, K., Badrawi, R., Chao, P., Franz, M., Grouios, C., Kazi, F., Lopes, C.T., *et al.* (2010). The GeneMANIA prediction server: biological network integration for gene prioritization and predicting gene function. Nucleic acids research *38*, W214-220.

Wu, T., Liu, Y., Wang, B., Sun, Y., Xu, J., Yuk-Wai, L.W., Xu, L., Zhang, J., and Li, G. (2016). The Use of Cocultured Mesenchymal Stem Cells with Tendon-Derived Stem Cells as a Better Cell Source for Tendon Repair. Tissue Eng Part A *22*, 1229-1240.

Yin, Z., Guo, J., Wu, T.Y., Chen, X., Xu, L.L., Lin, S.E., Sun, Y.X., Chan, K.M., Ouyang, H., and Li, G. (2016). Stepwise Differentiation of Mesenchymal Stem Cells Augments Tendon-Like Tissue Formation and Defect Repair In Vivo. Stem cells translational medicine *5*, 1106-1116.

Yu, H., Cheng, J., Shi, W., Ren, B., Zhao, F., Shi, Y., Yang, P., Duan, X., Zhang, J., Fu, X., *et al.* (2020). Bone marrow mesenchymal stem cell-derived exosomes promote tendon regeneration by facilitating the proliferation and migration of endogenous tendon stem/progenitor cells. Acta biomaterialia *106*, 328-341.

Zhang, B., Luo, Q., Deng, B., Morita, Y., Ju, Y., and Song, G. (2018a). Construction of tendon replacement tissue based on collagen sponge and mesenchymal stem cells by coupled mechano-chemical induction and evaluation of its tendon repair abilities. Acta biomaterialia *74*, 247-259.

Zhang, C., Zhang, E., Yang, L., Tu, W., Lin, J., Yuan, C., Bunpetch, V., Chen, X., and Ouyang, H. (2018b). Histone deacetylase inhibitor treated cell sheet from mouse tendon stem/progenitor cells promotes tendon repair. Biomaterials *172*, 66-82.

Zhao, B., Wei, X., Li, W., Udan, R.S., Yang, Q., Kim, J., Xie, J., Ikenoue, T., Yu, J., Li, L., *et al.* (2007). Inactivation of YAP oncoprotein by the Hippo pathway is involved in cell contact inhibition and tissue growth control. Genes & development *21*, 2747-2761.